

POLITECNICO DI TORINO

Master of science thesis in Energy and Nuclear Engineering

A.a 2021/2022



Development of anode-supported Solid Oxide Cell: cell modelling and experimental analysis

Relatore:

Santarelli Massimo

Candidato:

Blanco Giulia

Correlatore:

Ferrero Domenico

Sommario

Abstract	4
List of figures	5
Symbols.....	6
Introduction	9
1.Climate change and current situation	11
1.1Effect of Covid-19 in the energy demand	11
1.2 Global warming and Energy transition.....	13
1.3 Possible future scenarios	17
1.4 The role of the hydrogen	21
2.Solid oxide fuel cell.....	27
2.1 Technologies and processes	27
2.2 Solid Oxide Fuel Cell configuration.....	33
2.3 Faraday's Law and Nerst Equation	36
2.4 Transport phenomena	39
2.5 Polarization curve.....	45
3 Electrochemical model for a solid oxide fuel cell.....	49
3.1 Gas diffusion model	49
3.2 Mathematical model.....	50
3.3 Solving procedure.....	55
4 Model validation	58
4.1Parametric study	58
4.2 Reference polarization curve.....	60
4.3 Sensitivity analysis.....	62
5 Aspen model.....	71
5.1 SOFC stack modeling.....	71
5.1 Anode side.....	73
5.2 Cathode side	76
5.3 Thermal Balance.....	76
5.4Aspen Results.....	79
6 Conclusion.....	82
References	83

Abstract

Solid oxide fuel cells are considered as one of the most promising types of fuel cell for since characterized by an high efficiency power generators. The main problem of this kind of fuel cell is the high temperature operation so many research efforts have been placed on the materials, cell and stack designs, and improvements in power density in order to lowering the operating temperature.

Since an accurate design of flow distributors can allocate the fuel and the air uniformly into the anode and the cathode for achieving consistent diffusion processes through porous electrodes. The use of computational fluid dynamics is fundamental to maximise the performance, reducing the number of experimental tests to be performed, and so making the work less costly and time-consuming.

The thesis work consists on the analysis of the diffusion of the fuel in the anode. Considering a 1D simulation models where the fuel cell is represented by ordinary differential equations and the variation of parameters along the other two directions are negligible.

A planar SOFCs is analysed, so the dimension is usually determined by the gaseous flow direction in the fuel cell. Measuring the gas diffusivity in an electrode is an important aspect since gas diffusivity correlates with both polarization loss and electrode parameters including porosity, thickness and tortuosity.

The electrochemical part of the model has been implemented in the software tool MATLAB. It allows determining the local current density and the distribution of gas species, obtain at the end a polarization curve. A fitting procedure is done, starting from data taken from literature as experimental dataset, until the experimental curve and the one obtained from the modal are similar.

After the theoretical description and the mathematical model carried out using MATLAB, the SOFC module is also built using Aspen Plus.

In this part a real application is considered so the SOFC is feed with biogas, that is a mixture of carbon dioxide and methane, the output of Aspen Plus are used as input for the MATLAB code to obtain the final results.

List of figures

Figure 1- Global CO2 emission[7].....	11
Figure 2- Share of the CO2 emission in several sector[7]	12
Figure 3 -Renewable energy source partition[8].....	13
Figure 4 -Global mean temperature difference[18].....	15
Figure 5-evolution of the global temperature[3]	16
Figure 6-Reducing emissions by 2050 through six technological avenue[22]	17
Figure 7--Possible future scenarios[4].....	18
Figure 8-Net zero emissions scenarios[6]	19
Figure 9-Achievement of emission reduction[18].....	20
Figure 10-Evolving hydrogen production [18].....	22
Figure 11-Colour code hydrogen production [23].....	23
Figure 12-Global installed stationary fuel cell capacity growth[21]	25
Figure 13-Fuel cell sales, by region of adoption, 2016-2020 [23]	26
Figure 14-SOFC cross section[34].....	29
Figure 15-SOFC layer components [35].....	30
Figure 16- Planar SOFC configuration[8]	34
Figure 17-Model configuration of SOFC anode[15]	36
Figure 18-Polarization curve of soec(a) and sofc(b)[25]	46
Figure 19- Polarization curves for a fuel cell	47
Figure 20-Tortuosity[32].....	59
Figure 21- Reference polarization curve	62
Figure 22-Fist fitting setup results.....	65
Figure 23-second fitting setup results.....	66
Figure 24-cases 12/13/14.....	67
Figure 25-case 13	68
Figure 26-case 14	68
Figure 27-Aspen model	73

Symbols

n	[mol/s]	Molar flow
I	[A]	Current
Z	[-]	Charge number
F	[C/mol]	Faraday constant
ϕ	[W]	Heat flux
W	[W]	Power
h	[J/kg]	Specific enthalpy
s	[J/kgK]	Specific entropy
T	[°C] or [K]	Temperature
p	[bar]	Pressure
l	[J/kg]	Specific work
q	[J/Kg]	Specific heat
Δg	[kJ/mol]	Giggs free energy variation
E	[V]	Nernst voltage
ν	[-]	Stoichiometric coefficient
R	[J/molK]	Universal molar constant of gas
A	[cm ²]	Area
i	[A/ cm ²]	Specific current
η	[-]	Efficiency
OCV	[V]	Open circuit voltage
ASR	[Ω cm ²]	Area specific resistance
V	[V]	Voltage
i_0	[A]	Exchange current
β	[-]	Symmetric factor
ρ	[kg/m ³]	Density
D_{eff}	[cm ² s ⁻¹]	Effective diffusion coefficient
D	[cm ² s ⁻¹]	Molecular bulk diffusion coefficient

ε	[-]	Porosity
τ	[-]	Tortuosity
R	[Ω]	Resistance
ρ	[Ωm]	Resistivity
V_{op}	[V]	Operational voltage
E_0	[V]	Gibbs voltage
V_{TN}	[V]	Thermoneutral voltage
G	[kg/s]	Mass flow rate
c_p	[kJ/kgK]	Specific heat
c	[]	concentration
MM	[g/mol]	Molecular mass
M	[g/mol]	Molar mass
Na	[Particle/mol]	Number of Avogadro
q_{e-}	[C]	Charge of an electron
y	[-]	Molar fraction
η_{act}	[V]	Activation overvoltage
η_{ohm}	[V]	Ohmic overvoltage
η_{conc}	[V]	Concentration overvoltage
α	[-]	Transfer coefficient
δ	[cm]	Thickness
V_i	[-]	Füller diffusion volume
FU	[-]	Fuel utilization
SC	[-]	Steam to carbon ration
λ	[-]	Fuel equivalent ration
l_a	[m]	Anode thickness
l_c	[m]	Cathode thickness
l_e	[m]	Electrolyte thickness
σ	[A]	Collision diameter
Ω_D	[-]	Collision integral
γ	[A/m ²]	Activation energy paramenter
E_{act}	[KJ/mol]	Activation energy

Introduction

Climate change requires urgent attention. If we continue to emit CO₂ at current levels, only ten years remaining in the global carbon budget before we reach the 1.5 °C threshold, emphasising the need for immediate action.

To this issue, governments are responding with increasingly ambitious decarbonisation targets. At the time of the 2019 UN Climate Summit, 66 countries had announced their intent to meet net-zero carbon emissions targets by 2050.

In the EU, regulation includes potential fines for failure to meet targets, and a Green Deal was recently announced to support the net-zero emissions target.

To decarbonize the energy system the four main actions needed are: improving energy efficiency, developing renewable energy sources, switching to low/zero carbon energy carriers, and implementing carbon capture and storage (CCS) as well as utilization (CCU).

This will radically change energy supply and demand. Transitioning towards a low-carbon economy will radically change the share of energy supply and require large scale investments.

The need for an energy transition is nowadays widely understood; however, the implications and challenges related to the use of the renewable energy sources that must be resolved are still significant. These technologies, such as wind power and solar energy, strongly dependent on atmospheric conditions and meteorological fluctuations.

This often leads to a mismatch between the demand and the production. To solve this problem the need of storage system and energy vectors such as hydrogen or electricity is fundamental.

Electrochemical systems, such as fuel cells, are alternative technologies for directly converting the chemical energy into electrical energy. Hydrogen has the potential to be a powerful enabler of this transition, as it offers a clean, sustainable, and flexible option due to its simple production using renewable or nuclear energy, water electrolysis, allows producing hydrogen without direct CO₂ emissions and greenhouse gas emission.

Among the several types of fuel cell, solid oxide fuel cells (SOFCs) are perceived to be the most viable candidates for future power plants due to their high efficiency and fuel flexibility. SOFC is a clean energy conversion device, which undergoes improvement of performance continuously. Accurate modeling of the mass transport is imperative for development of better fuel cell designs.

The aim of this work is to model using MATLAB the diffusion of the fuel inside the electrodes, focusing on the anode side, since these phenomena are strictly related to the operating performances of the cell.

1. Climate change and current situation

1.1 Effect of Covid-19 in the energy demand

The Covid-19 pandemic had far-reaching impacts on energy demand in 2020, reducing global CO₂ emissions by 5.1%. However, the world has experienced an extremely rapid economic recovery since then, driven by unprecedented fiscal and monetary stimulus and a fast – although uneven – roll-out of vaccines. The recovery of energy demand in 2021 was compounded by adverse weather and energy market conditions, which led to more coal being burnt despite renewable power generation registering its largest ever annual growth.

Emissions increased by over 2.0 Gt from 2020 levels. This puts 2021 above 2010 as the largest ever year-on-year increase in energy-related CO₂ emissions in absolute terms. The rebound in 2021 more than reversed the pandemic-induced decline in emissions of close to 1.9 Gt experienced in 2020. CO₂ emissions in 2021 rose to around 180 megatons (Mt) above the pre-pandemic level of 2019.[7]

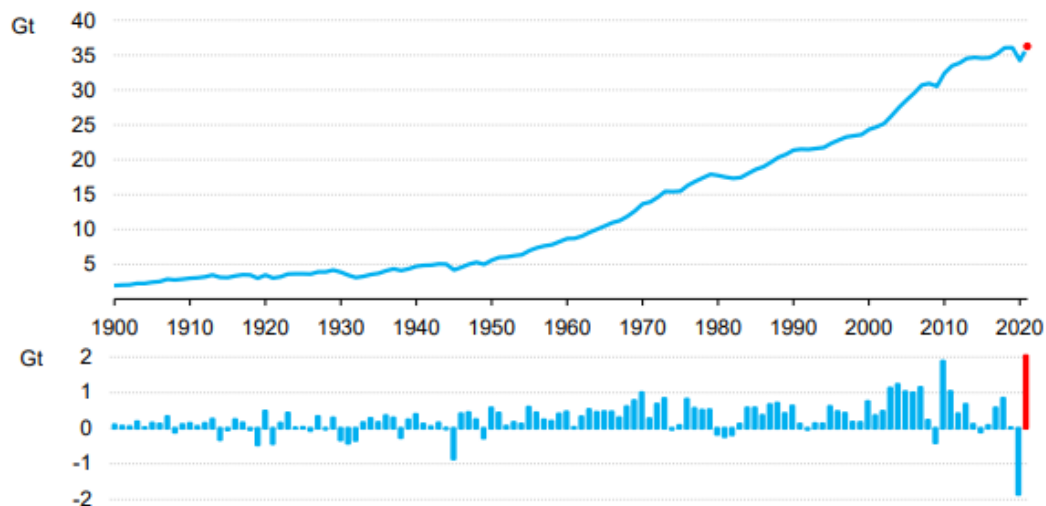


Figure 1- Global CO₂ emission[7]

The biggest increase in CO₂ emissions by sector in 2021 took place in electricity and heat production, where they jumped by more than 900 Mt. This accounted for 46% of the global increase in emissions, since the use of all fossil fuels increased to help meet electricity demand growth. Global CO₂ emissions from the buildings and industry sectors rebounded back to their

2019 levels, driven by increases in both advanced economies and emerging market and developing economies. Transport was the only sector in which global CO2 emissions remained well below 2019 levels.[7]

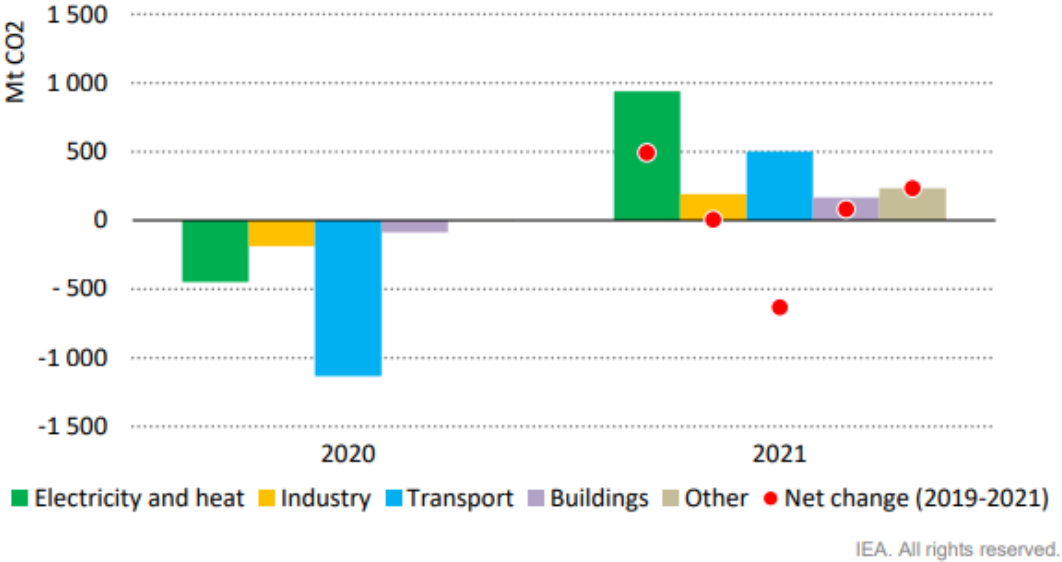


Figure 2- Share of the CO2 emission in several sector[7]

The recourse to coal-fired electricity generation in 2021 was compounded by record high natural gas prices.

Despite the rebound in coal use, renewable energy sources and nuclear power provided a higher share of global electricity generation than coal in 2021.

Renewable energy use increased 3% in 2020 as demand for all other fuels declined. The primary driver was an almost 7% growth in electricity generation from renewable sources. Long-term contracts, priority access to the grid, and continuous installation of new plants underpinned renewables growth despite lower electricity demand, supply chain challenges, and construction delays in many parts of the world. Accordingly, the share of renewables in global electricity generation jumped to 29% in 2020, up from 27% in 2019. Bioenergy use in industry grew 3%, but was largely offset by a decline in biofuels as lower oil demand also reduced the use of blended biofuels.[8]

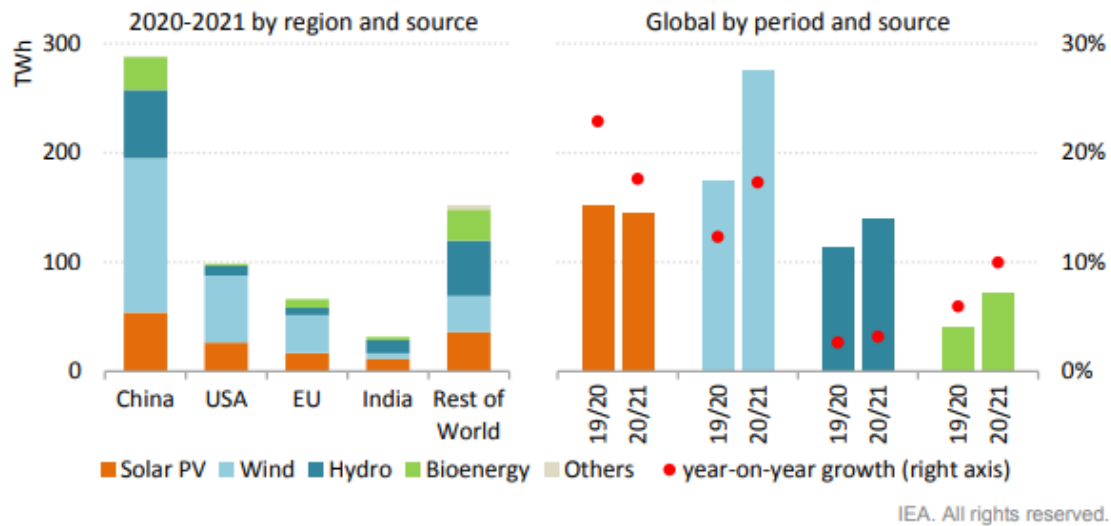


Figure 3 -Renewable energy source partition[8]

1.2 Global warming and Energy transition

Compounding crises underscore the pressing need to accelerate the global energy transition. Events of recent years have accentuated the cost to the global economy of a centralised energy system highly dependent on fossil fuels. Oil and gas prices are soaring to new highs, with the crisis in Ukraine bringing new levels of concern and uncertainty.

The COVID-19 pandemic continues to hamper recovery efforts, while citizens worldwide worry about the affordability of their energy bills. At the same time, the impacts of human caused climate change are increasingly evident around the globe. The Intergovernmental Panel on Climate Change (IPCC) warns that between 3.3 and 3.6 billion people already live in settings highly vulnerable to climate change.

Short-term interventions to ameliorate immediate challenges must be accompanied by a steadfast focus on a successful energy transition in the medium and long term. Governments today shoulder the challenging task of tackling seemingly opposing agendas of energy security, resilience, and affordable energy for all. In the face of uncertainty, policy makers must be guided by the overarching goals of arresting climate change and ensuring sustainable development.[22]

Climate change is increasing the frequency and intensity of extreme weather events such as heat waves, droughts, floods and tropical cyclones, aggravating water management problems, reducing agricultural production and food security, increasing health risks, damaging critical infrastructure and interrupting the provision of basic services such water and sanitation, education, energy and transport.[1]

2011-2020 was the warmest decade recorded, with global average temperature reaching 1.1°C above pre-industrial levels in 2019. Human-induced global warming is presently increasing at a rate of 0.2°C per decade.

An increase of 2°C compared to the temperature in pre-industrial times is associated with serious negative impacts on to the natural environment and human health and wellbeing, including a much higher risk that dangerous and possibly catastrophic changes in the global environment will occur.

For this reason, the international community has recognised the need to keep warming well below 2°C and pursue efforts to limit it to 1.5°C.

The main driver of climate change is the greenhouse effect. Some gases in the Earth's atmosphere act a bit like the glass in a greenhouse, trapping the sun's heat and stopping it from leaking back into space and causing global warming.

Many of these greenhouse gases occur naturally, but human activities are increasing the concentrations of some of them in the atmosphere, in particular:

- carbon dioxide (CO₂)
- methane
- nitrous oxide
- fluorinated gases

CO₂ produced by human activities is the largest contributor to global warming. By 2020, its concentration in the atmosphere had risen to 48% above its pre-industrial level (before 1750).

Other greenhouse gases are emitted by human activities in smaller quantities. Methane is a more powerful greenhouse gas than CO₂ but has a shorter atmospheric lifetime. Nitrous oxide, like CO₂, is a long-lived greenhouse gas that accumulates in the atmosphere over decades to centuries. Non-greenhouse gas pollutants, including aerosols like soot, have different warming and cooling effects and are also associated with other issues such as poor air quality.[2]

The gap between aspiration and the reality in tackling climate change remains as significant as ever, despite mounting evidence of the harm that climate change is causing. Negative effects of climate change are becoming more evident year by year. Yet global energy-related CO₂ emissions, despite levelling off periodically, have risen by 1% per year on average over the last decade.[18]

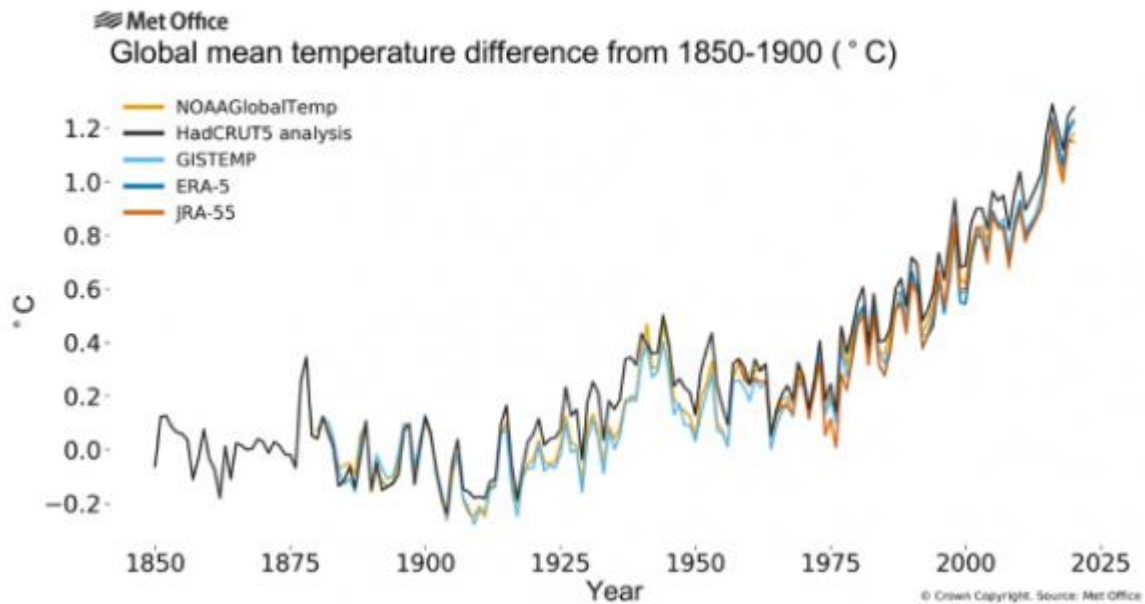


Figure 4 -Global mean temperature difference[18]

The year 2020 was one of the three warmest on record, and rivalled 2016 for the top spot, according to a consolidation of five leading international datasets by the World Meteorological Organization (WMO). A naturally occurring cooling climate phenomenon, La Niña, put a brake on the heat only at the very end of the year.

All five datasets surveyed by WMO concur that 2011-2020 was the warmest decade on record, in a persistent long-term climate change trend. The warmest six years have all been since 2015, with 2016, 2019 and 2020 being the top three. The differences in average global temperatures among the three warmest years – 2016, 2019 and 2020 – are indistinguishably small. The average global temperature in 2020 was about 14.9°C, 1.2 (± 0.1) °C above the pre-industrial (1850-1900) level.[19]

Temperature is just one of the indicators of climate change. The others are: greenhouse gas concentrations; ocean heat content; ocean pH; global mean sea level; glacial mass; sea ice extent and extreme events.[19]

Under the 2015 Paris Agreement, countries agreed to cut greenhouse gas emissions with a view to ‘holding the increase in the global average temperature to well below 2°C above pre-industrial levels and pursuing efforts to limit the temperature increase to 1.5°C above pre-industrial levels’.

To answer the question of how close we are to 1.5°C of warming, we need to first be clear about how both terms are defined in this Special Report. The choice of pre-industrial reference period, along with the method used to calculate global average temperature, can alter scientists’ estimates of historical warming by a couple of tenths of a degree Celsius.

In this report, warming is defined as the increase in the 30-year global average of combined air temperature over land and water temperature at the ocean surface. The 30-year timespan accounts for the effect of natural variability, which can cause global temperatures to fluctuate from one year to the next. In the decade 2006–2015, warming reached 0.87°C (±0.12°C) relative to 1850–1900, predominantly due to human activity increasing the amount of greenhouse gases

in the atmosphere. Given that global temperature is currently rising by 0.2°C ($\pm 0.1^{\circ}\text{C}$) per decade, human-induced warming reached 1°C above pre-industrial levels around 2017 and, if this pace of warming continues, would reach 1.5°C around 2040.

While the change in global average temperature tells researchers about how the planet as a whole is changing, looking more closely at specific regions, countries and seasons reveals important details. Since the 1970s, most land regions have been warming faster than the global average, for example. This means that warming in many regions has already exceeded 1.5°C above pre-industrial levels. Over a fifth of the global population live in regions that have already experienced warming in at least one season that is greater than 1.5°C above pre-industrial levels.[3]

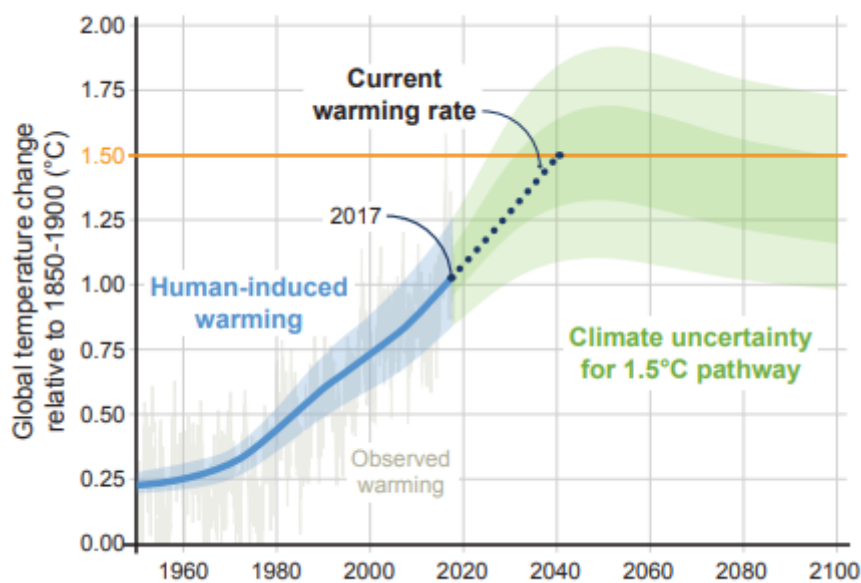


Figure 5-evolution of the global temperature[3]

Some 80% of the global population lives in countries that are net energy importers. With the abundance of renewable potential yet to be harnessed, this percentage can be dramatically reduced. Such a profound shift would make countries less dependent on energy imports through diversified supply options and help decouple economies from wide swings in the prices of fossil fuels.[22]

The 1.5°C Scenario outlined in the 2021 WETO envisions six technological avenues of an energy transition compatible with meeting the 1.5°C Paris climate goal:

1. **Renewables:** Renewable electricity generation sources such as solar PV, wind etc., and the direct use of renewable energy, such as solar thermal and biomass.
2. **Energy conservation and efficiency:** Measures to reduce energy demand and increase the energy efficiency of end-use applications, including structural changes (e.g. relocation of steel production with direct reduced iron, a modal shift in transport) and circular economy practices (e.g. alternative cement materials).

3. Electrification of end-use sectors: Direct use of clean electricity in transport and heat applications.

4. Hydrogen and its derivatives: Direct use of clean hydrogen (predominantly green hydrogen) along with synthetic fuels (green ammonia and methanol) and clean hydrogen-based feedstocks.

5. Carbon capture and storage (CCS): The carbon captured and stored from point-source fossil fuelbased and other emitting processes, mainly in industry. 6. Bioenergy coupled with carbon capture and storage (BECCS) and other carbon removal measures: Bioenergy coupled with carbon is captured and stored: in electricity, heat generation and industrial process (e.g. cement kilns and chemical production). Pursuing these six technological avenues at a rapid pace would result in significant emission reductions between today and 2050, paving the way to a net zero carbon world by mid-century.[22]

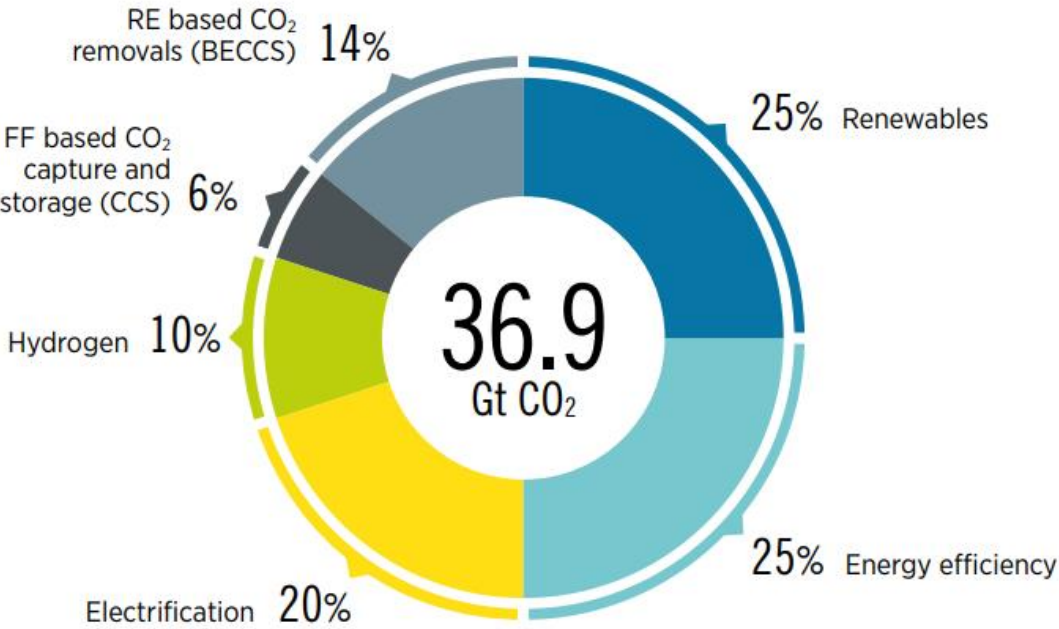


Figure 6-Reducing emissions by 2050 through six technological avenue[22]

1.3 Possible future scenarios

In a momentous period for the future of energy and emissions, the uses several long-term scenarios to illustrate the choices that face the world’s decision makers in the run-up to the crucial 26th Conference of the Parties (COP26) in November and beyond. A key variable in determining where the world goes from here is action taken by governments.

The main scenarios in this Outlook are:

- **Net Zero Emissions by 2050 Scenario (NZE)**, which sets out a narrow but achievable pathway for the global energy sector to achieve net zero CO2 emissions by 2050.

- **Announced Pledges Scenario (APS)**, which assumes that all climate commitments made by governments around the world, including Nationally Determined Contributions (NDCs) and longer term net zero targets, will be met in full and on time.

- **Stated Policies Scenario (STEPS)**, which reflects current policy settings based on a sector-by-sector assessment of the specific policies that are in place, as well as those that have been announced by governments around the world.[4]

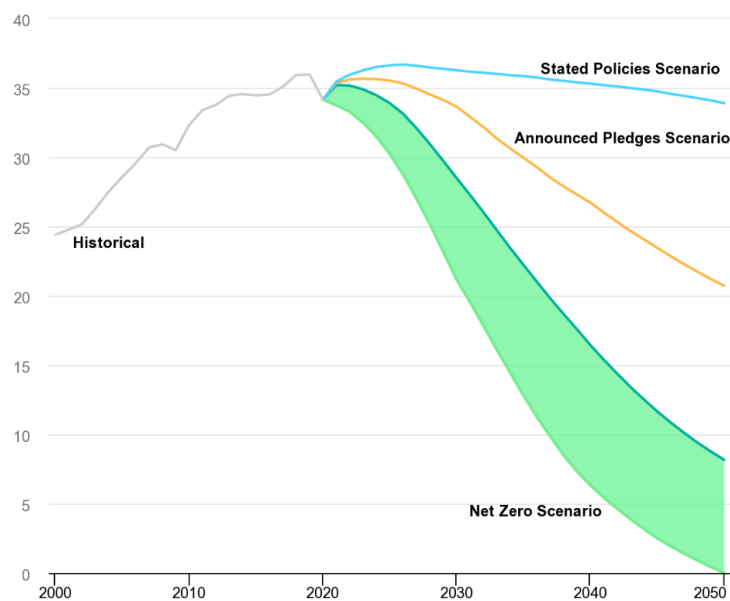


Figure 7--Possible future scenarios[4]

The path to net-zero emission is narrow: staying on it requires immediate and massive deployment of all available clean and efficient energy technologies.

Emissions reductions from the energy sector are not limited to CO2: in our pathway, methane emissions from fossil fuel supply fall by 75% over the next ten years as a result of a glob.

Reaching net zero by 2050 requires further rapid deployment of available technologies as well as widespread use of technologies that are not on the market yet. Major innovation effort must occur over this decade in order to bring these new technologies to market time.

The biggest innovation opportunities concern advanced batteries, hydrogen electrolysers, and direct air capture and storage. Together, these three technology areas make vital contributions the reductions in CO2 emissions between 2030 and 2050 in our pathway. [5]

In 2020, renewable electricity generation rose ~7%, with wind and solar PV technologies together accounting for almost 60% of this increase. The share of renewables in global electricity generation reached almost 29% in 2020, a record annual increase of two percentage points.

However, the drop in electricity demand caused by the Covid-19 slowdown in economic activity and mobility is a key reason for this record.

Renewable power deployment as a whole still needs to expand significantly to meet the Net Zero Emissions by 2050 Scenario share of more than 60% of generation by 2030. Yearly generation must increase at an average rate of nearly 12% during 2021-2030, almost twice as much as in 2011-2020.[6]

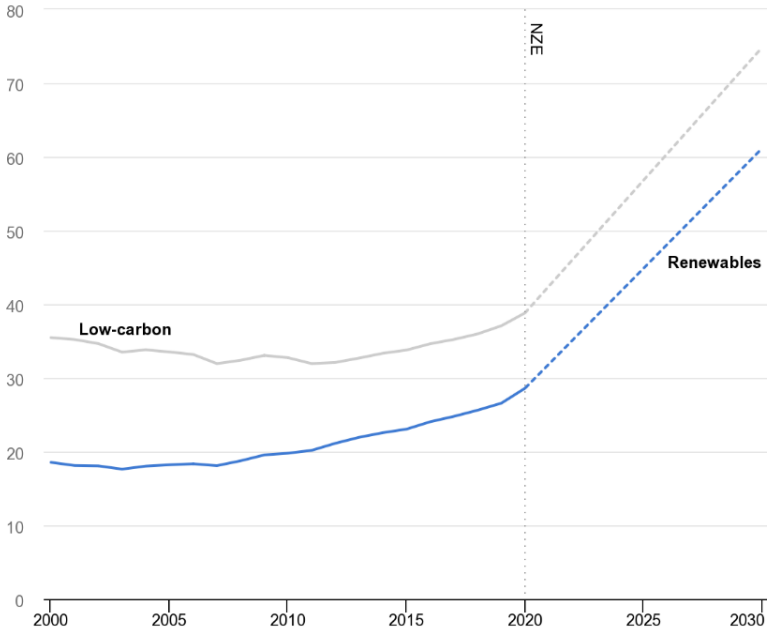


Figure 8-Net zero emissions scenarios[6]

Energy efficiency improvements must be scaled up rapidly and substantially. Energy efficiency and renewable energy are the two key solutions to enable the global energy transformation.

Of all energy sources in the electricity sector, only the use of renewables expanded in 2020, despite economic disruptions caused by Covid-19. Renewables-based electricity generation increased by 7.1% (a record 505 TWh) – almost 20% higher than average annual percentage growth since 2010.

Solar PV and wind each accounted for about one-third of total 2020 renewable electricity generation growth, with hydro representing another 25% and bioenergy the remainder. The first annual decrease in electricity demand since the financial crisis of 2008, combined with record PV and wind capacity additions in 2020, prompted the renewables share in total electricity generation to increase a record two percentage points. The share of renewables in the global electricity supply reached 28.6% in 2020, the highest level ever recorded.

Renewable power generation needs to continue expanding almost 12% annually over 2021-2030 to meet the Net Zero level. Despite record renewable capacity additions, generation growth was still significantly below the necessary level in 2020. Much faster deployment of all renewable

technologies will be needed to put the world on track with the Net Zero Emissions by 2050 Scenario.[6]

There are two general approaches to reducing emissions to zero: completely decarbonising all energy and industrial processes so that no CO₂ is emitted at all (the “zero” emissions approach), and offsetting any remaining emissions through the use of CDR to achieve net-zero emissions (the “net-zero” emissions approach). Examples of CDR include reforestation, afforestation, direct air capture, enhanced weathering and bioenergy CCS.[19]

It shows the relative contributions in four categories:

- 1) Renewable energy, including direct uses of renewable energy (e.g., biofuels, solar thermal), renewable power and both direct (e.g., EVs, heat pumps) and indirect electrification (e.g., green hydrogen, synthetic fuels);
- 2) Energy efficiency, including structural changes (e.g., circular economy, modal shifts) and behavioural changes (e.g., flying less);
- 3) Carbon management solutions, including CDR (e.g., reforestation, direct air capture), bio-energy with carbon capture and storage (BECCS), CCS, and carbon capture, utilisation and storage (CCUS) (including blue hydrogen);
- 4) Nuclear energy.[19]

To achieve this goal the hydrogen play an important role.

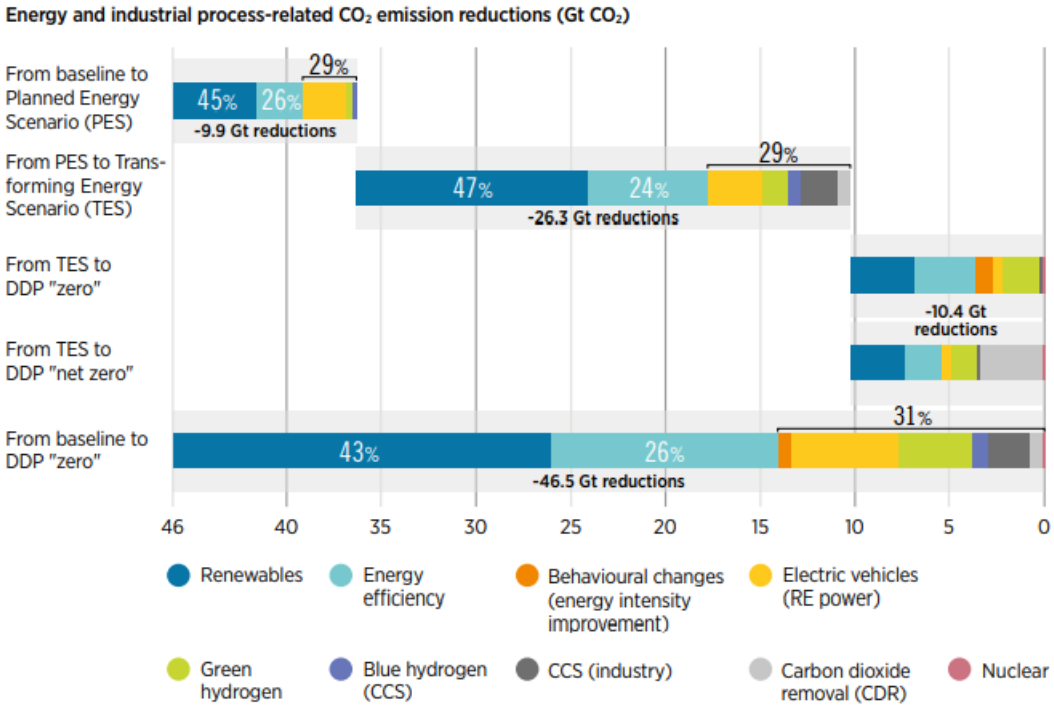


Figure 9-Achievement of emission reduction[18]

1.4 The role of the hydrogen

The increase of renewable electric energy production is crucial for replacing fossil fuels in transport, industrial and residential sectors. In this scenario, the development of suitable electric energy storage system is crucial in order to handle the unpredictability and the fluctuations typical of some renewable energy sources, such as wind and solar.

In this framework, one of the most attractive technologies is represented by hydrogen, when coupled with electrolyser, fuel cells and gas storage technologies. The basic principle of this technology lies in the use of the excess renewable electricity to produce hydrogen, using an electrolyser driven by renewable electricity. The produced hydrogen can be stored in suitable (pressurized tanks, metal hydrates, liquefied hydrogen, etc.) and subsequently supplied to a fuel cell to produce electricity, when the user demand is higher than the renewable production.

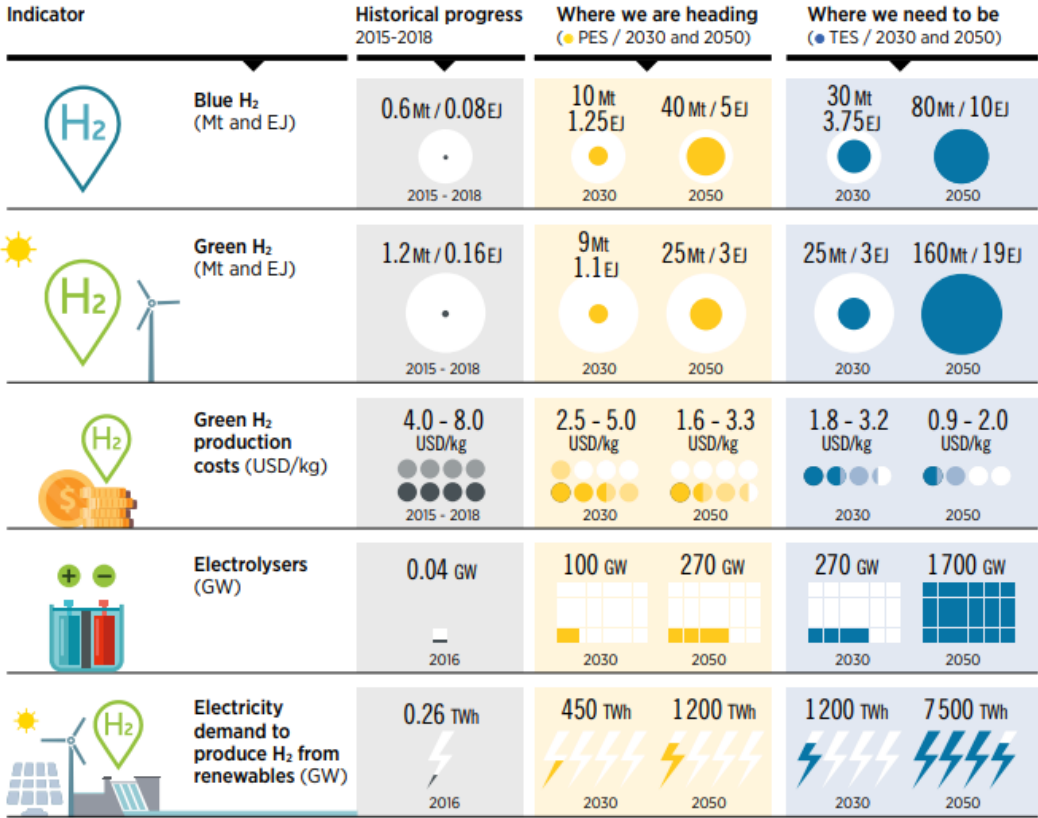
By coupling a reversible fuel cell with a photovoltaic (PV) or a wind turbine (WT) system, the fluctuations of the production of electricity can be limited thanks to the conversion into hydrogen. That solution, also called “green hydrogen production” allows one to store energy when renewable electricity production is higher than user demand and vice versa.[9]

Because hydrogen can be stored or used in a variety of sectors, converting electricity to hydrogen can help with the matching of variable energy supply and demand, both temporally and geographically, alongside alternatives such as pumped-storage hydropower, batteries and grid upgrades. If renewable power generation becomes sufficiently cheap and widespread, it can be used not only to provide low-carbon electricity, but also to create low-carbon hydrogen that can displace fossil fuels in transport, heating and industrial raw materials, and indeed almost any application not susceptible to electrification. All this makes hydrogen one of a suite of technologies that work well together to support the growth of low-carbon energy at the level of the overall energy system.[21]

Hydrogen can offer a solution for types of energy demand that are hard to directly electrify. Today almost all of this hydrogen comes from fossil fuels or from electricity generated by fossil fuels, with a high carbon footprint. Green hydrogen is produced by renewable electricity through electrolysis, and costs are falling fast. Green hydrogen will become cost competitive with “blue” hydrogen (produced from fossil fuels combined with carbon capture and storage [CCS]) in the next few years in locations with favourable low-cost renewable electricity.

Hydrogen can be processed further into hydrocarbons or ammonia, which can then help reduce emissions in shipping and aviation. The natural gas industry is also looking at hydrogen as a promising solution for greening the gas system and extending the life of existing infrastructure. However, this approach must be viewed with caution in light of unclear prospects of actually being able to significantly reduce emissions of the gas system and the potential to lock in carbon-intensive infrastructure.

A hydrogen commodity trade is nascent, but hydrogen could become the clean energy vector that makes it possible to tap into ample remote, low-cost renewable energy resources – a development that could have important geopolitical implications as well as further accelerating the demand for renewable power generation. [18]



Based on IRENA analysis

Figure 10-Evolving hydrogen production [18]

A colour-code system is commonly used to refer to different hydrogen production methods. Most hydrogen today is “grey” hydrogen, which is produced using fossil fuels, notably through steam methane reforming of natural gas or gasification of coal.⁷ These fossil fuel-based production methods, which account for 95% of today’s hydrogen supply, result in a substantial CO₂ footprint and are not compatible with moving towards net zero emissions.[23]

	GREY HYDROGEN	BLUE HYDROGEN	GREEN HYDROGEN
Process	Reforming or gasification	Reforming or gasification with carbon capture	Electrolysis
Energy source	Fossil fuels 	Fossil fuels 	Renewable electricity 
Estimated emissions from the production process ^a	Reforming: 9 - 11 ^b Gasification: 18 - 20	0.4-4.5 ^c	0

Note: a) CO_{2-eq}/kg = carbon dioxide equivalent per kilogramme; b) For grey hydrogen, 2 kg CO_{2-eq}/kg assumed for methane leakage from the steam methane reforming process. c) Emissions for blue hydrogen assume a range of 98% and 68% carbon capture rate and 0.2% and 1.5% of methane leakage.

Figure 11-Colour code hydrogen production [23]

Two main routes are under consideration to replace grey hydrogen with a clean form of production: green and blue hydrogen.

Green hydrogen production is fully consistent with the net zero route. It relies on technologies that have long been well known, based on water electrolysis powered by renewable electricity. Currently, hydrogen production from renewable sources is limited, but this is set to change with the global focus on its potential.

Blue hydrogen is produced from fossil fuels with CCS. Retrofitting CCS to grey hydrogen production facilities would allow continued use of these assets with lower greenhouse gas emissions. However, blue hydrogen relies on fossil gas, which brings risks of upstream or midstream leakages of methane, a much more potent greenhouse gas than CO₂. Blue hydrogen can thus yield very low greenhouse gas emissions, only if methane leakage emissions do not exceed 0.2%,⁸ with close to 100% carbon capture.[23]

Hydrogen holds long-term promise in many sectors beyond existing industrial applications. The transport, buildings and power sectors all have potential to use hydrogen if the costs of production and utilisation develop favourably relative to other options. The complex processes involved in developing and deploying hydrogen, however, mean that carefully crafted policy support will be critical.[21]

Power generation offers many opportunities for hydrogen and hydrogen-based fuels. In the near term ammonia could be co-fired in coal-fired power plants to reduce CO₂ emissions. Hydrogen

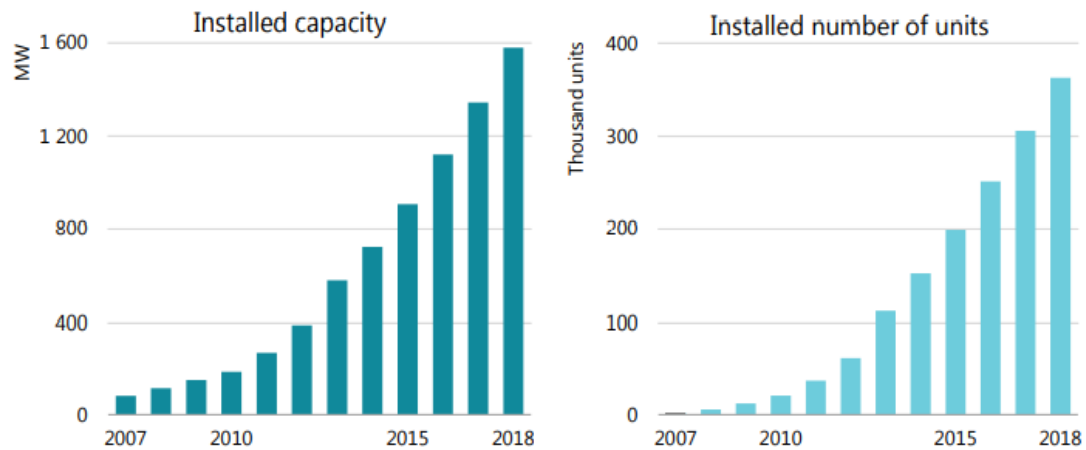
and ammonia can be flexible generation options when used in gas turbines or fuel cells. At the low capacity factors typical of flexible power plants, hydrogen costing under USD 2.5/kg has good potential to compete. Key low-carbon competitors for such services include natural gas with CCUS and biogas. In the longer term, hydrogen can play a role in large scale and long-term storage to balance seasonal variations.[21]

Fuel cells are a further option to convert hydrogen into electricity and heat, producing water and no direct emissions. Fuel cell technologies for stationary power applications Various fuel cell technologies exist for stationary power applications:

1. Polymer electrolyte membrane fuel cells (PEMFCs) operate at relatively low temperatures (below 100°C) and have a quick start-up time. They require, however, a pure hydrogen stream, or an external reformer if natural gas is used as fuel. PEMFCs are used today as micro co-generation units, operating with natural gas or LPG in residential buildings.
2. Phosphoric acid fuel cells (PAFCs), based on phosphoric acid as electrolyte, are used today as stationary power generators with outputs in the 100–400 kW range. In addition to electricity, they also produce heat at around 180°C, with potential uses for space and water heating.
3. Molten carbonate fuel cells (MCFCs) and solid oxide fuel cells (SOFCs) operate at higher temperatures, 600°C and 800–1 000°C respectively, which allow them to run on different hydrocarbon fuels without the need for an external reformer to produce hydrogen first. MCFCs are used in the MW scale for power generation (due their low power density, resulting in a relatively large size). The produced heat can be used for heating or cooling purposes in buildings and industrial applications.

SOFCs have similar application areas, often at smaller scale in the kW range, such as micro co-generation units or for off-grid power supply.[21]

Global installed stationary fuel cell capacity has been rapidly growing over the last ten years, reaching almost 1.6 GW in 2018, although only around 70 MW uses hydrogen as fuel; most of the existing fuel cells today run on natural gas.



Sources: E4tech (various years), *The Fuel Cell Industry Review*; S&P Global Platts (2018), *World Electric Power Plants Database*.

Figure 12-Global installed stationary fuel cell capacity growth[21]

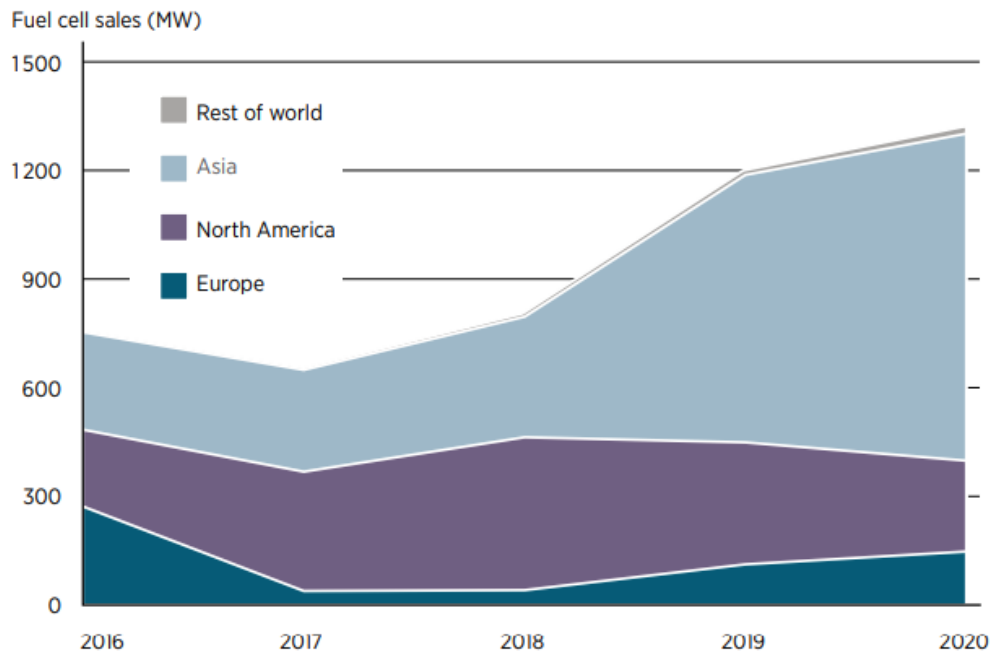
The provision of back-up power and off-grid electricity is today often still dominated by diesel generators. Fuel cells represent a possible alternative, in many cases reducing local air pollution as well as the need for imported diesel. Fuel cell systems, relying on bottled hydrogen, methanol or ammonia as fuel, offer an alternative to diesel generators or battery systems.

Compared to battery systems, fuel cells can operate in environments from -40°C to 50°C without the need for any cooling. (It has been also reported that compared to diesel generators, PV systems and batteries, fuel cells and their fuel appear less attractive to thieves.) Fuel cell systems, relying on bottled hydrogen, methanol or ammonia as fuel, offer an alternative to diesel generators or battery systems.

They can be manufactured with electronics industry techniques, and installed quickly and on a modular basis in densely populated areas. They run quietly without NOx emissions and provide resilience against power grid outages by using the natural gas grid, thus avoiding the need for on-site fuel storage.

The modular nature of fuel cells means that they lend themselves to real-time monitoring and servicing of components without downtime, which fits well with the trend towards more digitalisation in operations and branding. To reduce emissions they could switch to be run on hydrogen in the future or fitted with CO2 capture if a system for collecting the CO2 were available, for example for geological storage.[21]

Fuel cells can be deployed in stationary applications (at large-scale power plants, for instance); they can also be used in transport applications, such as fuel cell electric cars, trucks, buses, forklifts, ferries and ships, and aircraft. Historically, most policy support for hydrogen went to fuel cell electric vehicles and hydrogen refuelling stations. Global shipments of fuel cells have grown at a relatively modest pace, however. In 2020, 1.3 GW of fuel cells were sold globally. Most of the capacity went into cars, buses and trucks in Asia; some 8 000 FCEVs were sold in. Although it is the highest number on record, the figure pales compared with the 3 million electric cars sold globally the same year.[23]



Source: E4Tech (2021).

Figure 13-Fuel cell sales, by region of adoption, 2016-2020 [23]

2. Solide oxide fuel cell

2.1 Technologies and processes

Clean, affordable, efficient, and sustainable are the key features of an excellent power generator. One example is a solid oxide fuel cell (SOFC), a power generator that produces electricity from an electrochemical reaction between a fuel and an oxidant. An electrochemical cell is a device able to both convert chemical energy into electrical one, fuel cell, and also to convert the electrical energy into chemical one, electrolyser.

SOFC is a cogeneration device equipped with high fuel flexibility that permits cheap, safe, and readily available fuels such as hydrocarbons, coal gas, biomass, hydrogen, and syngas. In addition, SOFC can reform hydrocarbon fuels internally and tolerate some degree of common fossil fuel impurities, such as ammonia and chlorides.

Some of the advantages of the SOFC are low carbon emissions, long-term stability, and high output efficiency. Nowadays, the three application segments of the SOFC industry include stationary, transportation, and portable applications.[8]

SOFCs use a solid ceramic electrolyte, such as zirconium oxide stabilised with yttrium oxide, instead of a liquid or membrane. Their high operating temperature means that fuels can be reformed within the fuel cell itself, eliminating the need for external reforming and allowing the units to be used with a variety of hydrocarbon fuels. They are also relatively resistant to small quantities of sulphur in the fuel, compared to other types of fuel cell, and can hence be used with coal gas.

A further advantage of the high operating temperature is that the reaction kinetics are improved, removing the need for a metal catalyst. There are however some disadvantages to the high temperature: these cells take longer to start up and reach operating temperature, they must be constructed of robust, heat-resistant materials, and they must be shielded to prevent heat loss.[24]

The high operating temperature in addition to being a cause of problems (mechanical and chemical stability of materials used, higher start-up times than in other cells) allows the realization of internal reforming reactions to the cell itself.

An essential aspect related to SOFC cells is also the wide possibility of using the heat produced by the electrochemical reaction, mainly linked to ohmic losses and those of activation of the electrodes. The heat produced is used to keep high the operating temperatures of the cell, to

preheat the cathodic reagent flow and to heat recovery for cogeneration uses. Electrical power and heat are the two useful products of a SOFC stack.

There are three different SOFC geometries of SOFC: planar, coplanar and micro-tubular. In the planar design, components are assembled in flat stacks where the air and hydrogen traditionally flow through the unit via channels built into the anode and cathode. In the tubular design, air is supplied to the inside of an extended solid oxide tube (which is sealed at one end) while fuel flows round the outside of the tube. The tube itself forms the cathode and the cell components are constructed in layers around the tube.[24]

The two main used configurations are planar and tubular. These two different configurations then have variants, for example exist planar cells with a circular disc shape fuelled with fuel in correspondence central axis, or square planar configurations in which the fuel is fed at the outer edges.

Tubular cells can be classified according to the size of the diameter. In both cases, in typical operating conditions a single cell is able to produce a lower amount of voltage so is fundamental to connect several cells in series.

Focusing on the planar configuration, the key requirements that a cell must have with planar configuration are:

- Good electrical characteristics: the configuration of the cell must be such as to reduce ohmic losses in the stack. Current flow paths in the components must be as short as possible.
- Good electrochemical characteristics: configuration must ensure high open circuit voltages and minimal losses due to polarization.
- Thermal management: refers to the fact that the configuration must be such to have a uniform temperature distribution in the cell.
- Good mechanical characteristics: mechanical resistance must be maintained suitable for manufacture, assembly and operation.

The fuel cell is made of four basic functional components, two porous electrodes: anode and cathode, a dense electrolyte (between anode and cathode) and the interconnector. Is able to conduct a complete redox reaction. The oxidation occurs at the anode side while the reduction at the cathode.

The electrode mechanisms are more complicated and composition, morphology and thickness of the electrodes have to be carefully optimised in order to obtain good performance. Whatever the nature of the electrolyte is, the phenomena that takes place in the electrodes, for example in a cathode, can be summarised as follows:

1. transport of electrons from the current collector to the reaction site through an electronic conductor;
2. electrochemical reaction at an electrochemically active site, a point where the reactive gas, the electronic conductor and the ionic conductor are present at the same time (three phase boundary, TPB);
3. transport of ions from the reaction site to the electrolyte through the ionic conductor.

An analogous framework holds for the anode. So, the electrode must be formed by a mixture of ionic conductor/electronic conductor materials, and porosities must be present in the structure so that the gas can reach the active sites. Two parameters are of great importance for good electrode performances: an efficient three-phase boundary area, that is the active area for the electrochemical reaction, and a high level of ionic and electronic conductivities.[30]

Hydrogen-rich fuel is supplied to the anode side of the SOFC and undergoes a process known as fuel oxidation, where H_2 is oxidised and release electrons. At the same time the O^{2-} that are produced at the cathode side, that is supplied with air or pure oxygen, achieved through the electrolyte that is an ion-conducting ceramic solid layer, the anode where the water is released.

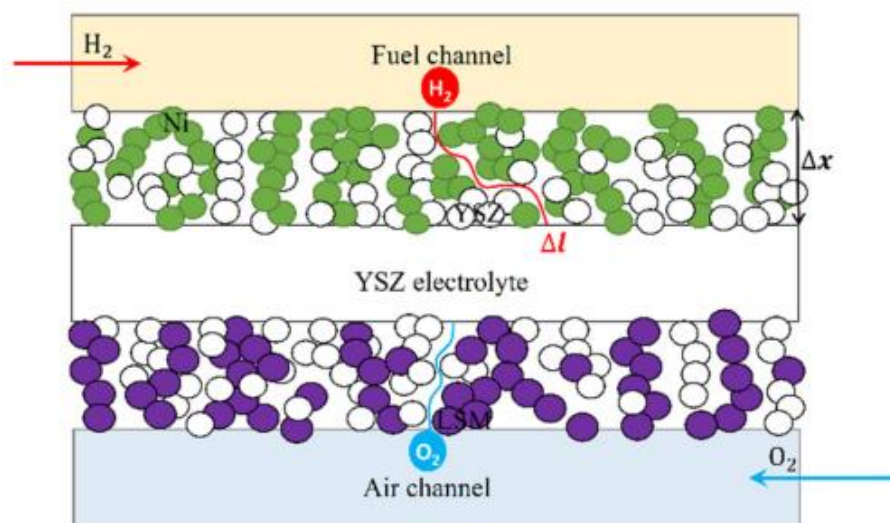
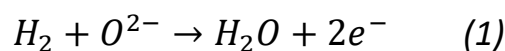
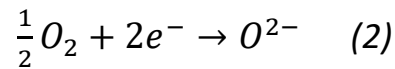


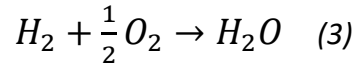
Figure 14-SOFC cross section[34]

The main reactions for anode and cathode of the SOFC, respectively are given in the following:





And the total reaction is as follows:



The released electrons would then travel through external circuit called interconnector that is used to electrically connect each single cells. Single cell comprises of anode, electrolyte and cathode. Interconnector are placed between single cells.

Several cells are connected in series forming the stack, because the voltage produce by a single cell is very low, in the order of magnitude of 0.8V, connecting in series a certain amount of cell a reasonable voltage is reached.

The interconnect acts also as a gas barrier separating the air on the cathode electrode and hydrogen on the anode electrode of adjacent repeating unit cell, to avoid the contact to the two gases that lead to the damage of the cell.

In the planar configuration to further avoid this leakages phenomenon a sealant, normally a glass sealant, due to the higher operating temperature, is used.

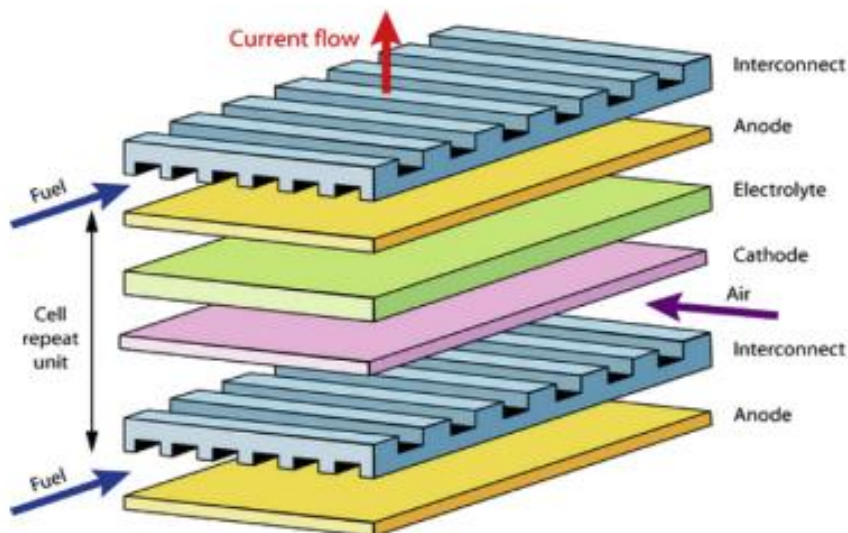


Figure 15-SOFC layer components [35]

These two semi-reactions generate a charge separation which leads to a voltage gradient. The difference between the anodic voltage gradient and the cathodic voltage gradient is defined as the voltage gradient of the cell. Considering the total number of cell, the voltage gradient of the stack is obtained.

The materials used for each component should have the following characteristics:

- Each component must have suitable electrical properties to achieve its function within the cell.
- Adequate chemical and structural stability at high temperatures during the operation of the cell as well as during the stages of manufacture.
- Minimal reactivity and diffusivity between the different components of the cell.
- Compatible thermal expansion between the various components of the cell.

Cathode

The cathode must have the following properties:

- High electronic conductivity.
- Chemical and structural stability during cell operation operations and during the manufacture of interconnections, the electrolyte layer and the anodic one
- Coefficient of thermal expansion compatible with the other components of the cell.
- Minimal reactivity and affinity with electrolyte and interconnects, components with which the cathode comes into contact.
- Sufficient porosity to facilitate molecular oxygen transport from the phase gaseous at the cathode-electrolyte interface.

The main material used for the cathode is the (LSM) strontium doped lanthanum manganite, that is a mixed ionic electronic conductor (MIEC) material. LSM is a p-type semiconductor, with good ionic and electronic conductivity. This component is characterized by a porous structure, to allow the mass transport of the reactant and of the product gases.

Electrolyte

The electrolyte must have some characteristics to be used successfully:

- It has to be dense.
- Must have proper composition to give good ion conduction to the operating temperatures.
- It must be thin to reduce ionic resistance.
- It must be extended as a surface to maximize current capacity.
- It must have thermal shock resistance.
- It must be easily machinable.
- Coefficient of thermal expansion similar to the other components.

The most effective material for the electrolyte is Y₂O₃-stabilized ZrO₂ (YSZ), Yttria stabilized zirconia materials. The SOFC operates at 600–1000°C where the ceramic electrolyte becomes conductive to oxygen ions, O²⁻, but not conductive to electrons. Due to the high operating temperatures the improvement of transport phenomena and the possibility to exploit non-precious catalysts is guaranteed.

At the same time the use of high-quality steel for auxiliary components is necessary. Other materials can be considered for the electrolyte layer with higher values of oxygen ion conductivity for example CeO₂, but they are less stable at low oxygen partial pressure.

Anode

The anode must have the following properties:

- High electronic conductivity.
- Chemical and structural stability during cell operation operations and during the manufacture.
- Coefficient of thermal expansion compatible with the other components of the cell.
- Minimal reactivity and affinity with electrolyte and interconnects, components with which comes into contact.
- Sufficient porosity to facilitate molecular oxygen transport from the phase gaseous at the cathode-electrolyte interface.

Typically, the anode is made of nickel/ yttria-stabilized zirconia (Ni/YSZ) cermet. Nickel has the functions of both catalyst and electronic phase. The anode should be porous, typical value are in the range of 15%-40%, for the same reason explained for the cathode.

Interconnector

In general terms, the interconnect has to meet the following demands:

- Excellent electrical conductivity. The acceptable area-specific resistance (ASR) level is considered to be below 0.1 Ωcm².
- Adequate stability in terms of dimensions, microstructure, chemistry and phases at operating temperature around 800°C in both oxidizing and reducing atmospheres.
- Excellent imperviousness for oxygen and hydrogen to prevent direct combination of oxidant and fuel during operation.
- Coefficient of thermal expansion matching those of electrodes and electrolyte.
- Low cost, as well as easy to fabrication and shaping.

Nowadays the material mainly used for the interconnector is Crofer 22 APU, that is a ferritic stainless steel doped with 22 wt% of chromium.

Sealant

Another fundamental aspect is related to the sealing material, to obtain gas-tightness and to prevent gas leakages. Material choice is not trivial, since must guarantee:

- Good adhesion with both ceramic electrodes and metallic interconnector, that are intrinsically different.
- The capability to join the different cell with the interconnector has to be guaranteed for different temperature ranges, so has to be able to sustain thermal cycles.
- Coefficient of thermal expansion similar to the other component.
- Good electronic resistivity

The state of art for the sealant is a glass-ceramic materials, typically an aluminium silicate.

2.2 Solid Oxide Fuel Cell configuration

Among the three different geometries of SOFC: planar, coplanar and micro-tubular. The two main used are the tubular and planar.

However, tubular SOFCs have been limited mainly due to practical fabrication procedures for such geometry into multiple assemblies. On the other hand, planar SOFC received much attention for their higher current density alongside straightforward and short-time fabrication process and assembly.

For single SOFCs, which are there is another distinction:

- Self-supported
- Externally-supported

As for the self-supported category, the layer that is the thickest functions as support for the structural cell; hence, it could be adopted as electrolyte supported, anode-supported or cathode-supported.

On the other hand, in that of externally-supported, thin layers of single cell are set upon substrate that is porous in nature. Both these two configurations possess benefits and drawbacks.

For electrolyte-supported SOFCs, elevated ohmic resistance from the thick electrolyte support contributes to low power density and is not commonly used. As an alternative, anode-supported SOFC is favoured due to its lower polarisation with additional improved electrochemical performance relative to cathode-supported SOFC.

Also, due to the demand for high power density at a lower operating temperature, SOFC designs primarily focus on a thin electrolyte film deposited on a porous electrode substrate. Nonetheless, anode, electrolyte, and cathode components in the SOFC design insinuate polarisation resistance due to electrode/electrolyte interfaces.[8]

Another possible option is the electrolyte (layer)-free fuel cell (EFFC). EFFC performs the fuel cell functions of converting H_2 and O_2 during cell operation, just like traditional SOFC. EFFC operates similarly to a single cell's electrochemical process, however, the geometry of the EFFC is significantly different from the conventional three-layer SOFC.

The structure of EFFC is a homomorphous layer constituted by a mixture of semiconductor and oxygen-ion, is considered as a single component cell that simultaneously serves as the electrodes and electrolyte.

One of the issues when utilising the EFFC is the risk of gas crisscross between the oxidant and fuel without dense electrolytes as the gas separator.

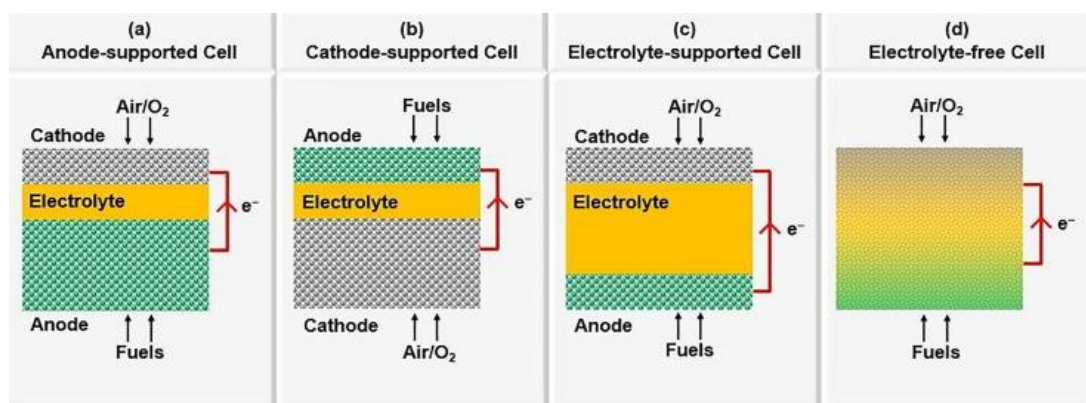


Figure 16- Planar SOFC configuration[8]

In the Figure 16 all the three configurations are represented. The support layer is the thickest one, so in the first is the anode, then cathode and the last in the electrolyte.

In the third picture electrolyte is the thickest and serves as the mechanical support for the whole cell. However, due to the high Ohmic resistance of the relatively thick electrolyte layer, the electrolyte supported design has been gradually replaced by the new electrode supported cells, in which one of the porous electrodes is the supporting structure.

Moreover, since cathode supported cell usually gives higher resistance, and is much harder to fabricate due to the mismatched thermal expansion coefficient of cathode support and functional layer, the anode supported cell (ASC) is the most widely accepted design in current SOFC research.[8]

To overcome the problems related to the high temperature operation of SOFC and enhance the performances, the research is focused on developing of new materials and configurations which

provides better or similar performance. An important aspect of reducing the operating temperature is the consequent reduction in the ionic conductivity of the electrolyte that led to higher ohmic overpotential.

The ohmic overpotential can be minimized by using electrode supported configuration of SOFC, in this way the thickness of the electrolyte is reduced. However, in electrode-supported cells, the contribution associated to the concentration overpotential, due to resistance to transport of reactants to the reaction sites becomes significant.

All these aspects point out that the thicknesses of different components of SOFC should be optimized in order to minimize both ohmic and concentration overpotentials to provides better performance.

The resistance to the flow of reactant species through the void spaces of the porous layers results in lower reactant concentration at the reaction sites. The mass transport limitation, so the concentration overpotential, is referred to loss in cell potential.

To minimize this concentration overpotential, that occurs mainly at higher current densities, an accurate determination of the rate of mass transport inside the porous electrodes is extremely important.

The rate of mass transport inside the porous electrodes of SOFC depends on the operating and design parameters such as temperature, pressure, fuel composition, pore size, porosity and tortuosity.[31]

The configuration of a SOFC anode can be simply modeled as shown in Figure-17. For modeling, the coupled electrochemical reaction and mass transfer in a composite anode and the reaction processes can be summarized as:

1. transport of reactant H_2 to the reaction sites through the pores of the anode and transport of O^{2-} from the electrolyte to the reaction sites through the ionic conducting particles;
2. electrochemical reaction of H_2 and O^{2-} to form H_2O and electrons at the active sites;
3. transport of electrons from the active sites to the current collector through the electronic conducting particles and transport of the H_2O product to the anode surface via the pores of the anode.

The configuration of the composite cathode of a SOFC also consists of both electronic and ionic conducting particles. Therefore, the mathematical model of the cathode side can be formed in the similar manner.[15]

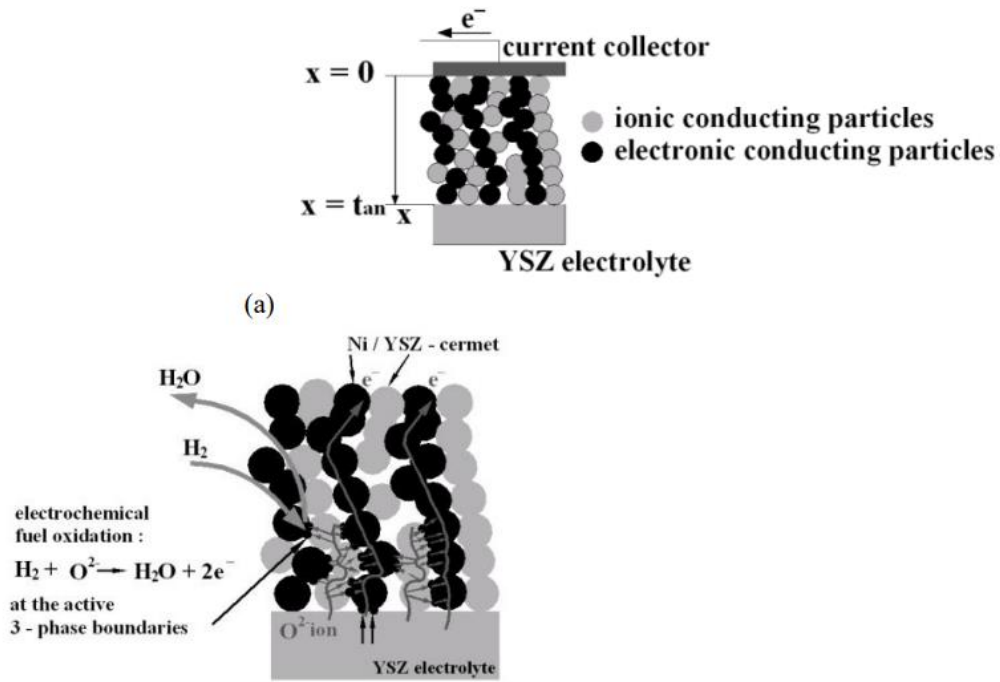


Figure 17-Model configuration of SOFC anode[15]

In this work the anode support cell is the one under study. In particular in the following chapters the modelling is done considering a circular shape.

2.3 Faraday's Law and Nerst Equation

The Faraday's Law of electrolysis expresses the magnitude of electrolysis effects. It quantifies the electric current produced by the flow of electrons:

$$\dot{n} = \frac{I}{Z_i F} \quad (4)$$

Where:

- \dot{n} is the molar flow, [mol/s] ;
- I is the current, [A];
- Z is the charge number [-], representing the number exchanged during the reaction (gained by reduction and delivered by oxidation);

- F is the Faraday constant, equal to 96485 [C/mol], and it is obtained multiplying the Avogadro constant $N_A = 6.02214076 \times 10^{23}$ [mol⁻¹] and the charge of an electron $q_{e^-} = -1.60217663 \times 10^{-19}$ [C].

$$F = N_A \cdot q_{e^-} \quad (5)$$

From the molar flow the mass flow G_i can be easily obtained using the molar mass M_i :

$$G_i = \dot{n}_i M_i \quad (6)$$

Going on with the thermodynamic and chemical analysis of the cell, another fundamental equation, called the Nernst equation, is introduced. The formula is obtained under the following hypothesis:

-The system is in equilibrium conditions, allowing the transition of state from the initial to the final conditions.

-Steady state conditions are considered; no dynamic behaviour is assumed.

And is written as:

$$E = -\frac{\Delta \widehat{g}_{react}}{ZF} \quad (7)$$

Where Δg_{react} is the Gibbs Free Energy and in the fuel cell mode operation is negative.

This equation is obtained considering the first and second laws of thermodynamic to the cell system. In case of fuel cell the power is produced so is positive and the Gibbs free energy is negative.

First law of thermodynamic:

$$\Phi - W_{el} - \left(\sum_{i=1}^n \dot{n}_i \bar{h}_i \right)_{product} + \left(\sum_{i=1}^n \dot{n}_i \bar{h}_i \right)_{reactant} \quad (8)$$

Second law of thermodynamic:

$$\frac{\Phi}{T} - \left(\sum_{i=1}^n \dot{n}_i \bar{s}_i \right)_{product} + \left(\sum_{i=1}^n \dot{n}_i \bar{s}_i \right)_{reactant} = 0 \quad (9)$$

These two equations can be rewritten divided by the molar flow of the fuel n_f all the terms, considering the stoichiometric coefficient ν_i , the molar specific heat and the molar work:

$$\nu_i = \frac{\dot{n}_i}{\dot{n}_f} \quad (10)$$

$$\bar{q} = \frac{\Phi}{\dot{n}_f} \quad (11)$$

$$\bar{l} = \frac{W_{el}}{\dot{n}_f} \quad (12)$$

So:

$$\bar{q} - \bar{l} - \left(\sum_{i=1}^n \dot{\nu}_i \bar{h}_i\right)_{product} + \left(\sum_{i=1}^n \dot{\nu}_i \bar{h}_i\right)_{reactant} \quad (13)$$

$$\frac{\bar{q}}{T} - \left(\sum_{i=1}^n \dot{\nu}_i \bar{s}_i\right)_{product} + \left(\sum_{i=1}^n \dot{\nu}_i \bar{s}_i\right)_{reactant} = 0 \quad (14)$$

The combination of these two equations allows the calculation of the open circuit voltage (OCV) that represents the voltage that would be measured during open circuit conditions, so without any current flow:

$$OVC_{fuel\ cell} = -\frac{\Delta g_{react}(T, p_0)}{ZF} + RT \ln \frac{\prod_i^{react} \frac{p_i^{\nu_i}}{p_0}}{\prod_i^{prod} \frac{p_i^{\nu_i}}{p_0}} \quad (15)$$

Where ν_i is the stoichiometric coefficient of the i -th species.

Since there is a direct connection between the partial pressure and the concentration of a chemical species the previous expression can be also written in the form:

$$OVC_{fuel\ cell} = -\frac{\Delta g_{react}(T, p_0)}{ZF} + RT \ln \frac{\prod_i^{react} \frac{c_i}{c_0}^{v_i}}{\prod_i^{prod} \frac{c_i}{c_0}^{v_i}} \quad (16)$$

Assuming that the gases are treated as ideal gas, the equation of the Nernst potential considering that the fuel cell works with hydrogen at the anode, oxygen at the cathode and producing water at the output, became:

$$OVC_{fuel\ cell} = -\frac{\Delta g_{react}(T, p_0)}{ZF} + RT \ln \left(\frac{p_{H_2} p_{O_2}^{1/2}}{p_{H_2O}} \right) \quad (17)$$

2.4 Transport phenomena

When the system is in operation, the cell works not as an open circuit but closed. The system is no longer in equilibrium conditions and the transport phenomena are the one that dominates.

The performance of a SOFC at high operating current densities is reduced mainly due to the mass transport losses, that is, the demand for reactants exceeds their capacity to diffuse through the porous anode to the reaction site at the anode–electrolyte interface.

The multi-component mass transport in SOFC anodes is also coupled with the bulk chemical reactions and the resulting diffusion and reaction time scales of different species dictate the limiting behaviour.

The three transport phenomena in the system are:

- The charge transfer;
- The charge migration;
- Molecular diffusion;

All these phenomena determine a voltage drop:

- Activation overvoltage;
- Ohmic overvoltage;
- Concentration overvoltage;

Each of these three terms can be expressed as a function of the current.

The voltage of the cell is obtained through the formula:

$$V_{cell} = OVC - \eta_{act} - \eta_{ohm} - \eta_{con} \quad (18)$$

The terms η_{conc} and η_{act} correspond respectively to the concentration and activation overpotentials both at the anode or cathode side. The ohmic term is expressed as the product of the ohmic resistance and the current.

The complete equation is:

$$V_{cell} = E_{i=0} + \eta_{conc}^{anode} + \eta_{conc}^{cathode} + \eta_{act}^{anode} + \eta_{act}^{cathode} + R_{ohm}i \quad (19)$$

with $E_{i=0}$ corresponds to the Open Circuit Voltage (OCV) expressed from the Nernst's equation:

$$E_{i=0} = E^0(T) + \frac{RT}{2F} \ln \frac{y_{H_2}^{TPBa, i=0} (y_{O_2}^{TPBa, i=0})^{0.5}}{y_{H_2O}^{TPBc, i=0}} \quad (20)$$

where $E^0(T)$ is the standard potential and y_j the partial pressures at OCV ($i = 0$) or under current ($i \neq 0$). The superscripts TPBa and TPBc denote the Triple Phase Boundaries at anode and cathode side.

The three-phase boundary (TPB) density is the most significant of all the microstructure parameters. This because the electrochemical reaction takes place in the TPBs where gas, electronic, and ionic phases meet. So, the TPB layer that is also called the active layer, is a mixed ionic and electronic conductor and is connected to the electrolyte.

Activation overpotentials

η_{act} is the activation overvoltage term, which represents the voltage loss induced by the electrochemical reactions occurring at the electrodes/electrolyte interfaces and so an energy barrier that must be overcome to activate the electrolysis process. The equation used in case of high-temperature cell to describe this phenomenon is the Butler-Volmer, this equation represents a standard model that describes the relation between the current density and the overvoltage in an electrode of a cell at the temperature of reacting chemical species:

$$i = i_0 \left[\exp \left(\beta \frac{F n_e \eta_{act}}{RT} \right) - \exp \left(\frac{-(1-\beta) F n_e \eta_{act}}{RT} \right) \right] \quad (21)$$

where i is the current density, β is the symmetric coefficient, i_0 is the exchange current, n_e is the number of electrons transferred per reaction.

The coefficient β is fraction of the activation energy, so is considered to be the fraction of the change in polarization that leads to a change in the reaction rate constant. The value for β varies from 0 to 1 and its value is usually 0.5 for the fuel cell application. The exchange current density is the forward and reverse electrode reaction rate at the equilibrium potential. A high exchange current density means that a high electrochemical reaction rate and good fuel cell performance can be expected.

When $\beta=0,5$:

$$i = 2i_0 \sinh \left(\frac{F n_e \eta_{act}}{2RT} \right) \quad (22)$$

So:

$$\eta_{act} = \frac{2RT}{F n_e} \sinh^{-1} \left(\frac{i}{2i_0} \right) \quad (23)$$

the general formula can be expressed for the two electrodes, considering the transport coefficient α for both anode and cathode:

$$i = i_{o,anode} \left\{ \exp \left(\frac{\alpha_a^{an} F \eta_{act}^{anode}}{RT} \right) - \exp \left(\frac{-\alpha_c^{an} F \eta_{act}^{anode}}{RT} \right) \right\} \quad (24)$$

$$i = i_{o,cathode} \left\{ \exp \left(\frac{\alpha_a^{cat} F \eta_{act}^{cathode}}{RT} \right) - \exp \left(\frac{-\alpha_c^{cat} F \eta_{act}^{cathode}}{RT} \right) \right\} \quad (25)$$

Where $i_{o,anode}$ and $i_{o,cathode}$ represent respectively the anode and cathode exchange current densities, defined as:

$$i_{o,anode} = \gamma_{an}(y_{H_2}(r))(y_{H_2O}(r)) \cdot \exp \left(\frac{-E_{act,an}}{RT} \right) \quad (26)$$

$$i_{o,cathode} = \gamma_{cat}(y_{O_2}(r))^{0.25} \cdot \exp \left(\frac{-E_{act,cat}}{RT} \right) \quad (27)$$

Where $E_{act,an}$ and $E_{act,cat}$ are respectively the activation energies of the anodic and cathodic reaction, while γ_{an} and γ_{cat} are parameters obtained from the fitting experimental data. Typical values for the γ_{cat} is $200 \cdot 10^9$ A/m², while in this thesis the γ_{an} used as adjustable parameter in the following chapter to fit the theoretical curve from the model with the experimental one. From literature typical value for the SOFC mode is $1.5 \cdot 10^9$ A/m².

In this case α is the transfer coefficient and can be expressed both for the anode and the cathode as:

$$\alpha_c^{an} = \beta \cdot \eta_{el,a} \quad \alpha_a^{an} = (1 - \beta) \cdot \eta_{el,a} \quad (28)$$

$$\alpha_c^{cat} = \beta \cdot \eta_{el,c} \quad \alpha_a^{cat} = (1 - \beta) \cdot \eta_{el,c} \quad (29)$$

With the symmetrical factor taken equal to 0.5:

$$\alpha_c^{an} = \alpha_a^{an} \quad \alpha_a^{cat} = \alpha_c^{cat} \quad (30)$$

The activation overpotentials can be derived from the equation:

$$\eta_{act}^{anode} + \eta_{act}^{cathode} = \frac{RT}{F} \sinh^{-1} \left\{ \frac{i}{2 \cdot i_{o,anode}} \right\} + \frac{RT}{F} \sinh^{-1} \left\{ \frac{i}{2 \cdot i_{o,cathode}} \right\} \quad (31)$$

The exchange current densities depend on the temperature according to an Arrhenius law and to the reactant/product concentrations in the neighbourhood of the active sites.

Ohmic overvoltage

η_{ohm} is the ohmic overvoltage term, depending on the ohmic resistance of both electrons and ions flows through all the components and the connectors. The equation adopted for calculating this term is:

$$\eta_{ohm} = iASR_{ohm} \quad (32)$$

where the area-specific ohmic resistance, ASR_{ohm} , is a semi-empirical function of the temperature and the materials.

The term $R_{ohm}i$ denotes the pure ohmic losses including all the layers: the ionic resistance of the electrolyte R_{el} and electronic resistances of both electrodes, for the cathode $R_{cathode}$ and for the anode R_{anode} .

The global contact resistances between the electrodes and the interconnects, R

$$R_{ohm} = R_{cathode} + R_{anode} + R_{el} + R_c \quad (33)$$

Where the structure of the R is :

$$R = \frac{\delta}{\rho} \quad (34)$$

Where ρ is the electrical conductivity of the material and δ the thickness of the considered layers. The contact resistance R_C is due to the current collection between electrodes and interconnects.

In planar configuration, electronic resistance of the electrodes is low compared to ohmic losses due to the electrolyte, so since the resistivity of the electrons is several orders of magnitude lower than the conductivity of the ions, this can be neglected.

Concentration overpotentials

η_{conc} is the concentration overvoltage term; it represents the voltage losses due to the mass transport phenomena occurring within the electrodes. The equation used to calculate this term is:

$$\eta_{con} = \frac{RT}{ZF} \ln \left(\frac{c_0}{c_\infty} \right) \quad (35)$$

where c_∞ is the concentration of the reactant before the diffusion layer, while c_0 is the one in the reactive zone.

This is the simplified equation that is valid for the anode as well as for the cathode. There is an equation that correlate the current density with the gradient of concentration in the thickness δ of the diffusion layer of the reactant.

$$i = \frac{ZFD \cdot (c_\infty - c_0)}{\delta} \quad (36)$$

Where D is the diffusion coefficient, that is widely explained in the following chapter. The limiting current density i_l is defined as the current density at which the concentration on the electrode surface is maximum so when c_0 is null:

$$i_l = \frac{ZFD(c_\infty)}{\delta} \quad (37)$$

Considering that:

$$\frac{i}{i_l} = \frac{c_\infty - c_0}{c_\infty} \quad (38)$$

The final expression is obtained:

$$\eta_{con} = \frac{RT}{ZF} \ln \left(1 - \frac{i}{i_l} \right) \quad (39)$$

Potential losses can arise in operation because of the electrode inability to maintain the fluid initial composition in the gas-phase surrounding the TPBs. These concentration overpotentials are expressed from the Nernst's equation. They can be caused by insufficient diffusion through the electrodes or insufficient steam flow rate introduced at the SOFC inlet.

$$\eta_{conc}^{anode} = \frac{RT}{2F} \ln \frac{y_{H_2O}^{TPBc(i=0)} \cdot y_{H_2}^{TPBc(i \neq 0)}}{y_{H_2O}^{TPBc(i \neq 0)} \cdot y_{H_2}^{TPBc(i=0)}} \quad (40)$$

$$\eta_{conc}^{cathode} = \frac{RT}{4F} \ln \frac{y_{O_2}^{TPBa(i \neq 0)}}{y_{O_2}^{TPBa(i=0)}} \quad (41)$$

The concentration of diffusion overvoltage is the one related to the diffusion of molecules in the electrodes. Mathematical models are needed to express this phenomenon. The three main equations are the Fick's law, the Stefan-Marxwell and the Dusty-Gas, that are analysed in the following chapter.

2.5 Polarization curve

Reliable and accurate SOFC modelling is critical to analyse and predict the output characteristics of SOFC systems under different operation conditions. The output V - I characteristics i.e., polarization curve, is used to illustrate the specific performance of SOFC systems.

Each of the three major losses contributes to the characteristic shape of the current–voltage (i - V) curve of the electrochemical cell. The figure below shows a typical i - V curve for water electrolysis and for a fuel cell. These voltage losses can result from cell polarization, leading to a loss in potential and the inability of cells to operate at the ideal voltage.

Under the standard condition with an environmental temperature of 298.15 K and atmospheric pressure of 1 atm, the standard electrode potential is 1.229 V, this value indicates the ideal electric potential energy.

In the case of water electrolysis, the current starts to flow across the cell above the thermodynamic electrolysis voltage of 1.23 V. Additional voltage is required to overcome the resistances discussed above. At low current densities, the voltage drops caused by ohmic resistances are small, and the reaction activation overvoltage accounts for the dominant part of the voltage drop.

The logarithmic shape of the polarization curve is attributed to the charge transfer phenomena at the anode and cathode. As the overvoltage increases further, the reaction activation barrier decreases, and the shape of the polarization curve becomes linear. This linear shape indicates that the ohmic resistance is now the key kinetic parameter of the cell.

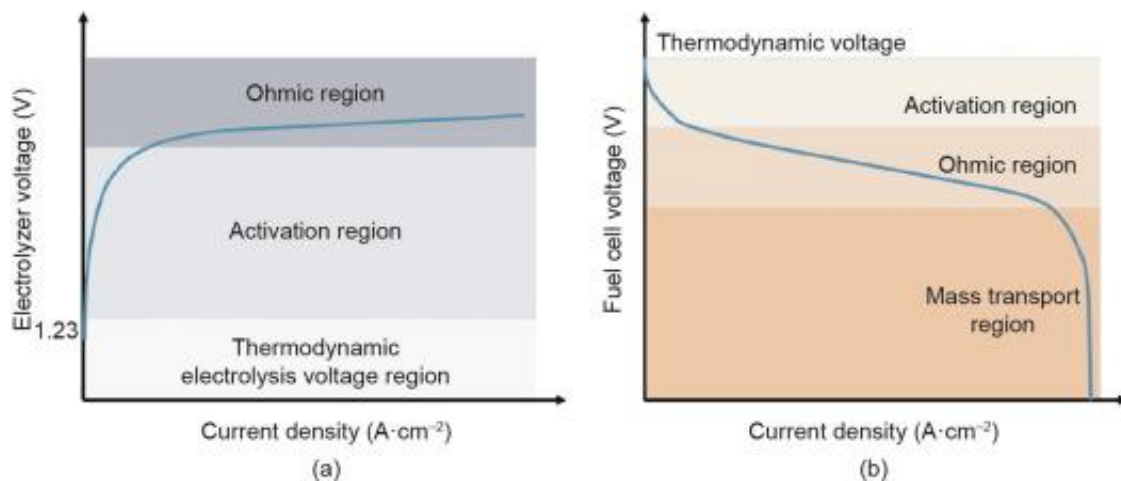


Figure 18-Polarization curve of soec(a) and sofc(b)[25]

In the case of the fuel cell, the activation resistances mostly affect the initial part of the curve, the ohmic resistances are mainly apparent in the middle section of the curve, and the concentration resistances are significant in the tail.

Although the reactions that occur in the two functioning technologies are reversible, the shapes of the $i-V$ curves are not the same: the $i-V$ curve for water electrolysis generally obeys the Butler–Volmer model even at very high overpotentials, while the $i-V$ curve for a fuel cell tends to show a constant value at high overpotentials due to the limitation in the mass transfer rate.[25]

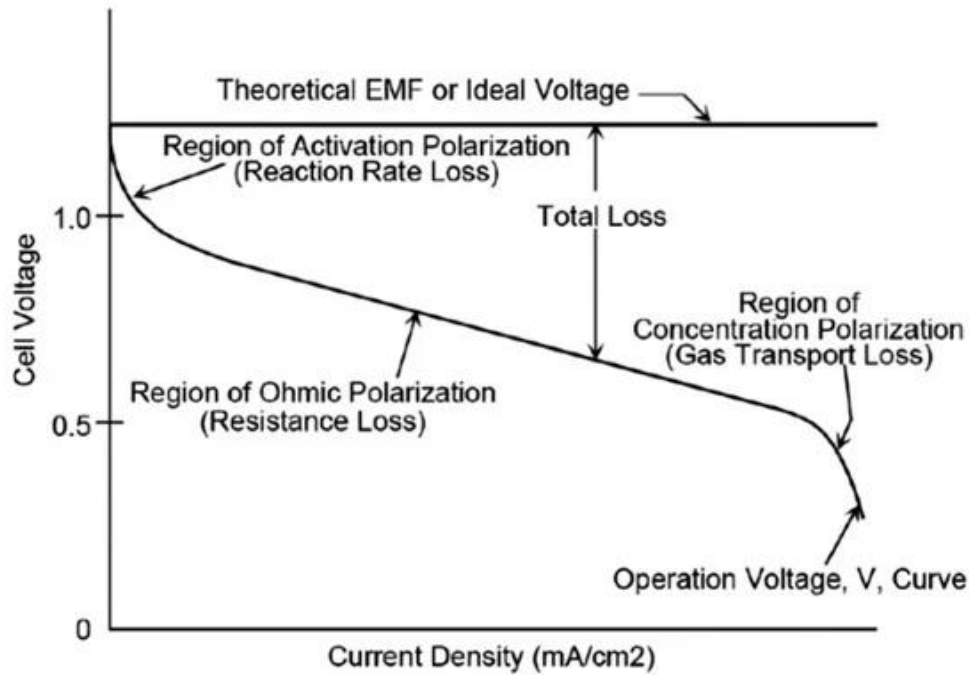


Figure 19- Polarization curves for a fuel cell

In the figures three distinct regions of a fuel cell polarization curve are well distinguishable:

- At low power densities, the cell potential drops as a result of the activation polarization.
- At moderate current densities, the cell potential decreases linearly with current due to ohmic losses.
- At high current densities, the cell potential drop departs from the linear relationship with current density as a result of a more pronounced concentration polarization.

The typical polarization curve of SOFC can mainly be divided into three different parts, i.e., activation polarization, concentration polarization, and ohmic polarization, upon which the specific output $V-I$ characteristics can be precisely described based on piecewise analysis.

Particularly, the activation polarization mainly represents the delayed chemical reaction from the activation barrier.

Meanwhile, the concentration polarization can effectively describe the concentration voltage drop result from mass transfer processes.

Lastly, the ohmic polarization indicates the ohmic loss which is mainly caused by various resistances, i.e., ionic resistance, electronic resistance, and contact resistance. Here, the accurate fitting of output polarization curve of SOFC is mainly depended on the accurate identification of several critical parameters in SOFC model.[27]

3 Electrochemical model for a solid oxide fuel cell

3.1 Gas diffusion model

As already seen the three types of energy losses associated with a fuel cell are the activation loss, concentration polarization, and Ohmic loss. Concentration polarization is caused by the mass transport phenomena, so induced by the pressure gradient due to limited transport rates of gaseous reactant and/or product species through SOFC electrode.

As the cell reaction proceeds, a concentration gradient of both the reactants and the products in the bulk electrolyte and on the electrode surface is formed. Due to this phenomenon the reactant molecules or the product molecules cannot reach or depart from the reaction sites. This induces a formation of an excess of product and a burnout of reactants on the electrode surface.

A thorough understanding of the gas transport mechanism along with an accurate calculation or measurement of concentration polarization at operating conditions is important for reducing polarization losses in SOFCs. The one-dimensional diffusion of gas fuel molecules in porous media involves molecular interactions between gas molecules as well as collisions between gas molecules and the porous media.[12]

Diffusion transport inside the porous medium has two components:

- Bulk molecular diffusion where molecular to molecular interaction dominates the transport, so is the phenomenon in case of large pore and high pressure.
- Knudsen diffusion where molecular to solid wall interaction dominates the transport, so when the mean free path of the molecules is higher than the pore size.

Several approaches have been developed to evaluate multicomponent porous media transport.

In general, models including Fick's model (FM), the Stefan–Maxwell model (SM) and the Dusty Gas model (DGM) are widely used to predict the concentration overpotential. Many researchers have concluded that among these three, the DGM is the most accurate and appropriate model to simulate gas transport phenomena inside a porous electrode such as SOFC electrodes. [14]

In 1D simulation models, the fuel cell is represented by ordinary differential equations and the variation of parameters along the other two directions are negligible. In planar SOFCs, the dimension is usually determined by the gaseous flow direction in the fuel cell. In the 1D, the parameters vary along a direction parallel to the axes of the gas channels for planar SOFCs. Gaseous compositions, flow rates, pressures and temperatures are averaged for each gaseous flow channels.[15]

In this work, a one-dimensional electrochemical model for a circular solid oxide cell operating in fuel cell mode is presented. The model has been developed considering the study of Laurencin et al. [28] and it has been implemented in MATLAB.

The model requires as input the voltage of the cell and the inlet flow rates of the gases entering and calculates as output the evolution of the molar flow rates of the chemical species on the electrodes by solving an implicit ODE equation obtained from the polarization equation.

The molar flow rates obtained are needed to calculate the local current density in the cell, the total current of the cell is calculated considering the total area of the cell. Combined together the voltage and the current the whole polarization of the cell is obtained.

3.2 Mathematical model

To simplify the model and calculations, the following hypothesis are considered:

- All gases involved are assumed to be ideal gases.
- The flow inside the channels and porous electrodes is assumed to be laminar.
- The electrochemical reactions are assumed to take place at the triple phase boundary (TPB).
- The electrodes are assumed to be homogeneous and isotropic media with porous microstructures.
- The effect of gravity is neglect.
- The system is considered isothermal and in steady state condition.
- The pressure drops are neglect.
- 1D circular geometry.
- Constant electrical potential.

The model assumes that the gases are distributed in parallel-flow arrangement, flowing from the centre of the circular cell to the border on both the electrodes.

Therefore, the system has a perfect circular symmetry, described by only one dimension, the radius (r); the inlet gases on both sides enter the system at $r = 0$ so at the centre of the cell and exit at $r = r_{\text{border}}$ where r_{border} corresponds to the radius of the cell. The cell radius is about 3.87 cm so the total area of the cell of 47cm^2 .

Reacting gases diffuse in the electrodes in the perpendicular direction respect to the radius so in the z direction, from the electrode surface to the TPB or from the TPB to the electrode surface; the TPB is assumed to be located at interface of both cathode/electrolyte and anode/electrolyte.

The concentrations of the chemical species at the TPB are used in the calculation of the concentration overpotentials. These concentrations are calculated by integrating the diffusion equations of the Dusty Gas Model from the electrode surface to the TPB.

Thanks to the assumption of the constant electrical potential, all the points in the electrode are assumed to be at the same potential, this means that the applied potential is not a function of the radius. This assumption is realistic considering that the electrodes are good electrical conductors.

The equation needed to solve the system are:

- Mass transfer.
- Gas flow along the anodic and cathodic channels.
- Mass transport in the porous electrodes.

Mass transfer

In this case the pressure drop along the gas channels is assumed negligible, so the atmospheric condition has been considered for the gas-phase pressure, this means that the value of the pressure is $P_T = 1$ atm.

Gas flow along the anodic and cathodic channels

For what concern the variation of molar fractions along the gas channel, this is caused by molar fluxes through the porous electrodes. This variation is calculated using the local mass balances, evaluated for each species along the channels, through the equation 40 in case of general planar configuration.

$$\frac{dn_i}{dx} = \gamma_i e N_i \quad (42)$$

Where n_i represents the molar flow rate in the channels for the specie i , N_i the flux through the electrode, e is the width of the gas channel and, γ_i is a stoichiometric coefficient that can assume the values +1 or -1, is equal to -1 for the reactant species and +1 for the product species.

Since the cell evaluated in this work are characterized by a circular shape the cylindrical coordinates should be considered, so the equations became the following ones considering the three different species, where the molar flow rates are calculated using the Faraday's law:

$$\frac{dn_{H_2(r)}}{dr} = -\frac{i(r)}{2F} 2\pi r \quad (43)$$

$$\frac{dn_{O_2(r)}}{dr} = -\frac{i(r)}{4F} 2\pi r \quad (44)$$

$$\frac{dn_{H_2O(r)}}{dr} = \frac{i(r)}{2F} 2\pi r \quad (45)$$

Where n_i denotes the molar flow rate expressed in mol/s on the surface of the electrode of the I specie and $i(r)$ is the local current density in A/cm².

Mass transport in the porous electrodes

In porous electrodes the main phenomenon considered is the diffusive flow, the viscous one, that is driven by the pressure gradient, is normally considered negligible. As already seen the three main equations used for model the diffusion effect are the Fick's law, Stefan-Maxwell or Dusty Gas Model.

The simplest among the three diffusion models is the Fick's law and is used in case of dilute or binary systems. The equation expresses the proportionality between the net flux and the gradient of the concentration of the corresponding species, through the effective diffusion coefficient D_i^{eff} of the species which takes into account of the composition of the gas mixture.

$$N_i = -\frac{P}{RT} D_i^{eff} \frac{dy_i}{dx} \quad (46)$$

The calculation of D_i^{eff} can be carried out following the equation 45.

$$D_i^{eff} = D_{bulk} \frac{\varepsilon_p}{\tau_p} \quad (47)$$

Where D_{bulk} is the diffusion coefficient in bulk condition so before any interaction of the gas species with the electrode, while ε_p and τ_p are respectively the porosity and tortuosity of the porous electrode.

The Stefan-Maxwell model is instead commonly used in case of multicomponent systems because it considers the molecular collisions among the different types of gas species.

The Dusty Gas Model is an extension of the Stefan-Maxwell equation accounting for friction between gas molecules and the porous medium, which is treated as an immobile "dusty gas" species.

The Dusty Gas Model further considers the interactions between the gas molecules and the solid pore surface leading to Knudsen diffusion. This model assumes the pore walls consist of large molecules that are uniformly distributed in space.

These pseudo 'dust' molecules also collide with real gas molecules, which leads to the Knudsen diffusion effect. Moreover, the fluxes due to pressure gradient are also taken into consideration.

Therefore, the mass transport through the porous electrodes has been described in the frame of the DGM model, by combining the Stephan-Maxwell and Knudsen diffusion:

$$\frac{N_i}{D_{i,k}^{eff}} + \sum_{j=1, j \neq i}^n \frac{y_j N_i - y_i N_j}{D_{i,j}^{eff}} = - \frac{P_T}{RT} \left(\frac{dy_i}{dx} \right) \quad (48)$$

Where y_i is the molar fraction of specie i . The effective Knudsen and binary diffusion coefficients, respectively $D_{i,k}^{eff}$ and $D_{i,j}^{eff}$, have been determined as a function of the electrodes microstructure parameters that are the mean pore radius \bar{r} , tortuosity τ and porosity ε . In porous media such as SOFC or SOEC electrodes, the following expressions are usually employed:

is the theoretical diffusion coefficient of species

$$D_{i,j}^{eff} = D_{i,j} \frac{\varepsilon_p}{\tau_p} \quad (49)$$

$$D_{K,i}^{eff} = D_{K,i} \frac{\varepsilon_p}{\tau_p} \quad (50)$$

In this work the binary coefficient D_{ij} is calculated using Chapman–Enskog relations:

$$D_{ij} = \frac{0.00266}{\sqrt{2}} \frac{[T^3(M_i+M_j)/M_iM_j]^{1/2}}{P\sigma_{ij}^2\Omega_D} \quad (51)$$

The pressure P is the total pressure of the mixture and T is one of the system, M_i represents the molecular weight of the species i and M_j of the species j , while the value σ_{ij} is the Lennard-Jones characteristic length and is obtained from the expression:

$$\sigma_{ij} = \frac{\sigma_i + \sigma_j}{2} \quad (52)$$

Where in this case σ_i and σ_j represent the Lennard-Jones potential.

The parameter Ω_D is the collision integral and is a dimensionless parameter calculated through this formula:

$$\Omega_D = \frac{A}{T_N^B} + \frac{C}{\exp(DT_N)} + \frac{E}{\exp(FT_N)} + \frac{G}{\exp(HT_N)} \quad (53)$$

In this expression, the coefficients have respectively these values:

A=1,06036; B=0,1561; C=0,193; D=0,47635; E=1,03587; F=1,52996; G=1,76474; H=3,89411.

The dimensionless temperature T_N is obtained considering the Boltzman constant k and the term ε_{ij} obtained from the characteristic Lennard-Jones energy of the species i according to:

$$\varepsilon_{ij} = (\varepsilon_i \varepsilon_j)^{1/2} \quad (54)$$

So:

$$T_N = \frac{kT}{\varepsilon_{ij}} \quad (55)$$

For what concern the Knudsen diffusion coefficient, can be assessed according to the kinetic theory of gases:

$$D_{K,i} = \frac{2}{3} \left(\frac{8RT}{\pi M_i} \right)^{1/2} \bar{r} \quad (56)$$

Where M_i denotes the molecular weight for the gas i and \bar{r} is the mean pore radius that in this case is assumed equal to 0.5 μm considering typical values founded in litterature.

Since both these two mechanisms are present when the gas diffuses inside the porous electrode, to consider both of them a single diffusion coefficient is evaluated combined together the previous two, using the Bosanquet formula the final diffusion coefficient is obtained for each molecular species:

$$\frac{1}{D_{(eff)}} = \frac{\tau}{\varepsilon} \left(\frac{1}{D_{i,j}} + \frac{1}{D_{K,i}} \right) = \frac{1}{D_{i,j}^{eff}} + \frac{1}{D_{K,i}^{eff}} \quad (57)$$

3.3 Solving procedure

Integrating the DGM the different molar fractions are obtained for all the species involved evaluated at the TPB of the electrodes. At the anode considering the hydrogen and the water, for the cathode the air and the nitrogen or in general the dilution stream.

The mass transfer process of H₂ in the porous electrode of the anode is by means of diffusion. Considering both Knudsen diffusion and molecular diffusion, the mass flux of hydrogen can be determined as express in the equation (56):

$$N_{H_2} = -\frac{P}{RT} \left(\frac{1}{D_{H_2,k}^{eff}} + \frac{1-\alpha y_{H_2}}{D_{H_2O-H_2}^{eff}} \right)^{-1} \left(\frac{dy_{H_2}}{dx} \right) \quad (58)$$

where $\alpha = 1 - (M_{H_2}/M_{H_2O})^{1/2}$; and M_{H₂} and M_{H₂O} the molecular weights of the hydrogen and water, respectively; and Deff_{H₂,k} and Deff_{H₂O-H₂} are the Knudsen diffusion coefficient of hydrogen and the binary diffusion coefficient of the mixture, respectively.

From this formula the expression of hydrogen molar fraction is obtained.

So as results at the anode side the solution gives the molar fraction for the hydrogen and the water.

The flux ratios at steady-state are determined by the stoichiometry of the reaction. Therefore:

$$N = N_{H_2} + N_{H_2O} = 0 \quad (59)$$

For equimolar counter-current:

$$N_{H_2} = -N_{H_2O} = \frac{i}{2F} \quad (60)$$

Where:

$$N_{H_2} = -D_{H_2}^{eff} \nabla c_{H_2} + c_{H_2} v \quad (61)$$

and :

$$N_{H_2O} = D_{H_2O}^{eff} \nabla c_{H_2O} + c_{H_2O} v \quad (62)$$

Where c express the concentration of the hydrogen and water.

In this case the two diffusion coefficients are expressed as:

$$\frac{1}{D_{H_2}^{eff}} = \frac{1}{D_{H_2,k}^{eff}} + \frac{1}{D_{H_2O-H_2}^{eff}} \quad (63)$$

$$\frac{1}{D_{H_2O}^{eff}} = \frac{1}{D_{H_2O,k}^{eff}} + \frac{1}{D_{H_2O-H_2}^{eff}} \quad (64)$$

Integrating for the anode side the equation (48), the molar fraction for the three streams at this side are obtained.

$$y_{N_2TPB}(r) = y_{N_2}(r) \cdot \exp(-k_1 l_{an}) \quad (65)$$

$$y_{H_2TPB}(r) = y_{H_2}(r) + k_2 l_{an} + \frac{k_3}{k_1} (y_{N_2in} - y_{N_2in} \exp(-k_1 l_{an})) \quad (66)$$

$$y_{H_2OTPB}(r) = y_{H_2O}(r) + k_4 l_{an} + \frac{k_5}{k_1} (y_{N_2in} - y_{N_2in} \exp(-k_1 l_{an})) \quad (67)$$

In this expressions l_{an} is the thickness of the anode and the coefficients k_i are expressed as:

$$k_1 = \frac{RT}{P} \left(\frac{N_{H_2}}{D_{N_2,k}^{eff}} + \frac{N_{H_2O}}{D_{H_2O-N_2}^{eff}} \right) \quad (68)$$

$$k_2 = \frac{RT}{P} \left(\frac{N_{H_2}}{D_{H_2,k}^{eff}} + \frac{N_{H_2O}}{D_{H_2O-H_2}^{eff}} \right) \quad (69)$$

$$k_3 = \frac{RT}{P} \left(\frac{N_{H_2}}{D_{H_2,k}^{eff}} - \frac{N_{H_2O}}{D_{H_2O-H_2}^{eff}} \right) \quad (70)$$

$$k_4 = \frac{RT}{P} \left(\frac{N_{H_2O}}{D_{H_2O,k}^{eff}} + \frac{N_{H_2O}}{D_{H_2O-H_2}^{eff}} \right) \quad (71)$$

$$k_5 = \frac{RT}{P} \left(\frac{N_{H_2O}}{D_{H_2O,N_2}^{eff}} - \frac{N_{H_2O}}{D_{H_2O-H_2}^{eff}} \right) \quad (72)$$

For what concern the cathode side, the transport of O_2 can be described by the self-diffusion mechanism es express in the formula (73):

$$\frac{dP_{O_2}}{dx} = - \frac{RTi}{4FD_{O_2}^{eff}P} (P - \delta_{O_2}P_{O_2}) \quad (73)$$

Where :

$$\delta_{O_2} = \frac{D_{O_2,i}^{eff}}{D_{O_2,i}^{eff} + D_{O_2-N_2}^{eff}} \quad (74)$$

The integration led to the expression for the oxygen molar fraction:

$$y_{O_2TPB}(r) = \frac{1}{\delta_{O_2}} + \left(y_{O_2}(r) - \frac{1}{\delta_{O_2}} \right) \exp \left(- \frac{RTl_{cat}\delta_{O_2}}{4FD_{O_2}^{eff}p} \right) \quad (75)$$

The solving procedure and the MATLAB code adopted is the one developed in the thesis [33]

4 Model validation

4.1 Parametric study

In a SOFC system, computer simulation based on theoretical modeling is known to be a very efficient method for predicting materials properties, reaction kinetics and unit cell performance. Different levels of model, depending on the objective, have been developed, each with different degrees of sophistication and detail.

Theoretical modeling of SOFC can be divided into two levels: macro and micro-scale. Detailed understanding of fluid and mass transport shows whether heat transfer can be obtained from macro-scale modeling. The effects of porosity change on reactant concentration and ohmic overpotentials could also be considered in the macro-scale modeling, but the activation overpotential must be treated as a property independent of the porosity, while the electrochemical reactions must occur only at the interface between electrode and electrolyte layers.

The macro-scale modeling is not a good predictor of the effect of electrode structure on the chemical reaction within SOFCs. Influence of the electrode structure on the reaction of kinetics at the three-phase boundary (TPB) has recently been included in micro-scale modeling of SOFCs. In literature for micro-scale modeling, the properties of porous electrodes and their effects on SOFC performance have been investigated from different aspects.[15]

The porous electrodes are responsible for the transport of gas species and charges and also for the removal of exhaust gases. So, the porous electrode must serve as media for the transport of gas, heat, ions, and electrons.

Parameters like tortuosity, porosity, and permeability are very important to determine the transport properties of the electrode. The gas transport is instead determined by intrinsic properties of the chemical species such as viscosity and diffusivity, which are related to the temperature and the gas composition.

The effective gas diffusion coefficient and effective charge conductivity are linked to all these parameters. The impact of variation of them has an effect on the SOFC performance such as fuel utilization, current density, activation overpotential and concentration overpotential.

The tortuosity τ is an intrinsic property of a porous material and is usually defined as the ratio between the shortest pathway through a porous media and the Euclidean distance between the starting and the ending point, so to the straight line between the two points, In this simplified system tortuosity is defined as the ratio of the length of the real diffusion patch, L_e , to the patch in the straight channel case, L_s .

$$\tau = \frac{L_e}{L_s} \quad (76)$$

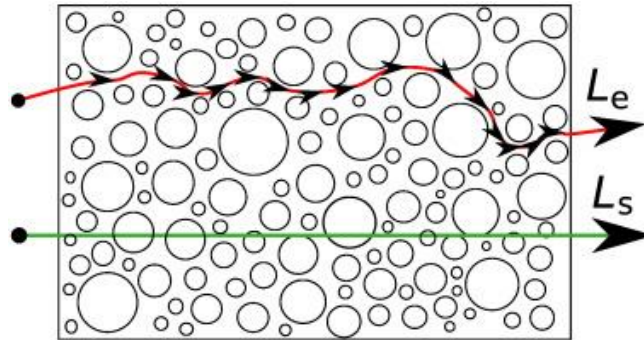


Figure 20-Tortuosity [32]

Tortuosity of the electrode mostly affect the limiting current density of a fuel cell electrode, this decreases with the increasing of the tortuosity. For most porous fuel cell electrodes, the typical value of tortuosity varies in the ranges from 2 to 25 and fuel cell performance can be improved by varying the tortuosity values in this range.

The porosity ε is defined as the fraction of the void space volume in the media and the total volume, so the bulk volume.

$$\varepsilon = \frac{V_{pore}}{V_{bulk}} \quad (77)$$

The use of thin nanostructured electrodes is highly recommended since only relatively low porosity is needed to achieve high SOFC efficiencies with such electrodes. The critical porosity is defined as the value where concentration polarization (CP) reaches a plateau and remains unchanged with further increase in porosity. Typically, critical porosity value for 10 nm thick electrodes is 0.15, followed by 0.4, and 0.7 for 100 nm, and 500 nm anodes, respectively. [12]

4.2 Reference polarization curve

To confirm the accountability of our numerical scheme and determine the goodness of the mathematical model implemented with MATLAB, we validated our results with available experimental data, comparing the two polarization curves. The predicted cell performance is compared with the experimental data found in the literature.

The scientific paper under evaluation is the ‘Experimental investigation of direct internal reforming of biogas in solid oxide fuel cells’.[29].

The performance of the cell is predicted when the cell is supplied with 50% H₂ and 50% CO₂, while operating at a temperature of 850°C and pressure of 1 atm. The oxidant used is the oxygen in the ambient air. The present model predictions agree well with the experimental results.

In ‘Experimental investigation of direct internal reforming of biogas in solid oxide fuel cells’ paper the behaviour of a planar SOFC fed by different mixture composition was investigated.

The fuel mixture are namely bio-methane and bio-hydrogen, the case of interested in the purpose of this thesis is only the bio-hydrogen, since the cell in this work is just feed by hydrogen at the anode side.

The composition of the bio-hydrogen is mixture of H₂ and CO₂, in general with a volumetric ratio of 50/50. In the paper several tests are done at different temperatures, but only the resulting curve at 850°C is taken under consideration, as already mentioned. The flows were:

- 500 Nml min⁻¹ for H₂,
- 500 Nml min⁻¹ for CO₂,
- The air flow was 1500 Nml min⁻¹.

As already mentioned, an Anode Supported Cell (ASC) was tested. The ASC used for the test was an 80 mm diameter anode supported cell with:

- 500 mm Ni/8YSZ of porous anode support, 10 mm of a denser Ni/8YSZ anode active layer,
- 5 mm 8YSZ of dense electrolyte,
- LSM/8YSZ double cathode layer with 15 mm LSM/8YSZ active layer and 20 mm pure LSM porous current collector layer.

Summary	
<i>Hydrogen flow rate [Nml min⁻¹]</i>	500
<i>Air flow rate [Nml min⁻¹]</i>	1500
<i>Diluted flow rate [Nml min⁻¹]</i>	500
<i>Temperature [K]</i>	1173
<i>Anode thickness [m]</i>	500 e-6
<i>Cathode thickness [m]</i>	35 e-6
<i>Electrolyte thickness [m]</i>	5 e-6

Table 1-Summary of input and properties of the cell

The curve is obtained interpolating the 30 points for the voltage and the current. The values for each point are:

Current [A]	Voltage [mV]
0,026	915,7
1,108	905,6
2,055	897,68
3,047	890,26
4,039	877,52
4,969	872,24
6,085	861,63
7,943	853,19
9,059	842,59
9,927	836,23
10,98	827,76
11,972	818,21
12,902	808,66
14,142	801,26
15,01	791,71
16,064	782,17
16,932	773,67
17,924	764,14
19,101	752,47
19,97	742,92
21,148	729,13
22,079	715,32
23,071	702,58
24,002	688,77
24,995	670,71
26,112	647,32
26,982	624,99
27,853	598,84
29,035	555,84
29,961	501,02

Table 2- Current and voltage values

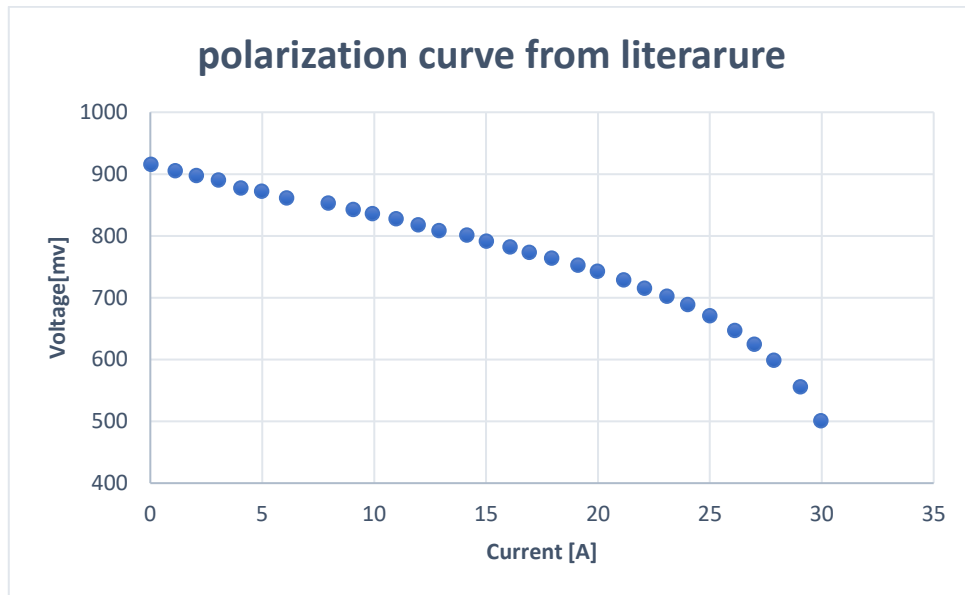


Figure 21- Reference polarization curve

This curve is used as a reference, varying the fitting parameters that are the tortuosity, the porosity, the ohmic resistance and the parameter related to the activation energy for the anode.

The MATLAB code is run using as input the same flow rate for the hydrogen, the air and diluted stream, considering a temperature of 1173 K that is the operating temperature of the cell.

Then the fitting parameters are changed until the curve results obtained from the model and the one from the experiment are similar. In this case the model can be considered able to reproduce a realistic polarization curve and the value obtained as used as input for the following section in the Aspen model.

4.3 Sensitivity analysis

Considering electrode porosity, reducing porosity can reduce the ohmic overpotential as more solid particles are available to facilitate the transport of electronic and ionic charges. In addition, the activation overpotential is also reduced with decreasing porosity due to the increase in reactive site.

However, the concentration overpotential increases with decreasing porosity due to diminishing of space available for gas transport. The combined effects of porosity on ohmic, activation, and

concentration overpotentials for minimization of the overall overpotential result in an optimal porosity for the electrode.

The effect of increasing porosity when fixed solid fraction of the electrode means that the particle radius of the electrode decreases. This results in the reduction of the active surface area available for the electrochemical reaction, so the reaction rate decreases resulting in an increase of the activation overpotential.

Moreover, the effective ionic and electron conductivities of the porous electrode decrease with the increase of porosity, which results in the increase of ohmic overpotential.

Although the concentration overpotential decreases with the increase of porosity due to the increased mass transport rates the cell performance decreases due to increased ohmic overpotential with porosity.

Another aspect is that an increase in porosity tends to smoothen the current density distribution. These observations can be explained by relating how porosity affects the effective ionic/electronic conductivities on the active reaction sites. The observed reduction in the average and maximum current density values with an increase in porosity can be attributed to the reduction in solid volume fraction, which results in less particle–particle contacts. This translates into a smaller number of active three phase boundary (TPB) for electrochemical reaction sites and, therefore, lowering the reaction rate for a given overpotential.

Additionally, the increased porosity also reduces the effective electronic and ionic conductivity due to reduced solid fraction available for electron or ion transport. Further, an increase in porosity results in a facilitation of reactants diffusion, which minimizes the reactants transport limitation under the interconnect region and helps smoothen the current density distributions [15]

Tortuosity, usually determined experimentally, is a key parameter that is valid only for specific materials and may change during operation conditions. In numerical analysis it is often used as a fitting parameter, correlated with calculation model and material.

An increased pore tortuosity is correlate to the fact that more gas can be transported to the reaction site and thus more ions and electrons are produced. Since the path for ion and electron transfer does not change, the lack of a transfer path led to the decrease of current density. So higher values of tortuosity can be used to calibrate the diffusion limitation.

The result further confirmed that a decreased pore tortuosity does not favour the electrochemical reactions and charge transfer. If handled improperly, the increase of the gas path leads to more open pores and less percolated ionic and electronic phases.

14 different cases changing the parameters are done to obtain a realistic representation of the curve, varying the porosity, tortuosity, the parameter P that is related to the activation energy γ_{act} and the ohmic resistance inside the respectively ranges.

The parameter P mainly affects the activation part of the polarization curve, while the ohmic resistance is the main responsible parameter for the linear trend of the curve that is related to the ohmic overpotential, changing it the curve is shifted up or down according to a decrease or an increase of its value.

The range selected for the porosity is from 0.3 and 0.15, a lower value of the porosity in not allows since the code gives as output an error due to the impossibility to converge. The value of

the tortuosity is selected between 3 and 10, also in this case for the same reason explained for the porosity, the tortuosity cannot be higher than 10. The ohmic resistance is varied between $0.110 \Omega/\text{cm}^2$ and $0.252 \Omega/\text{cm}^2$. The last is the parameter related to the activation energy γ_{act} , denominates as P that in general for an SOFC is equal to 1.5, that is varied between this value and 1.3.

A first setup is done considering four cases with these characteristics:

Case1:

T[°C]	Por.	Tort.	Rohm[Ω/cm^2]	P	Lcat[m]	Lan[m]	Lelct[m]
1173	0.3	3	0.152	1.5	35 e-6	550 e-6	5 e-6

Case2:

T[°C]	Por.	Tort.	Rohm[Ω/cm^2]	P	Lcat[m]	Lan[m]	Lelct[m]
1073	0.2	4	0.152	1.3	35 e-6	500 e-6	5 e-6

Case3:

T[°C]	Por.	Tort.	Rohm[Ω/cm^2]	P	Lcat[m]	Lan[m]	Lelct[m]
1173	0.15	6	0.252	1.5	35 e-6	500 e-6	5 e-6

Case4:

T[°C]	Por.	Tort.	Rohm[Ω/cm^2]	P	Lcat[m]	Lan[m]	Lelct[m]
1173	0.15	8	0.152	1.4	35 e-6	500 e-6	5 e-6

The results obtained plotting these curves are summarized in the fig-22, where the dots are representing the reference polarization while the other curves the four cases analysed.

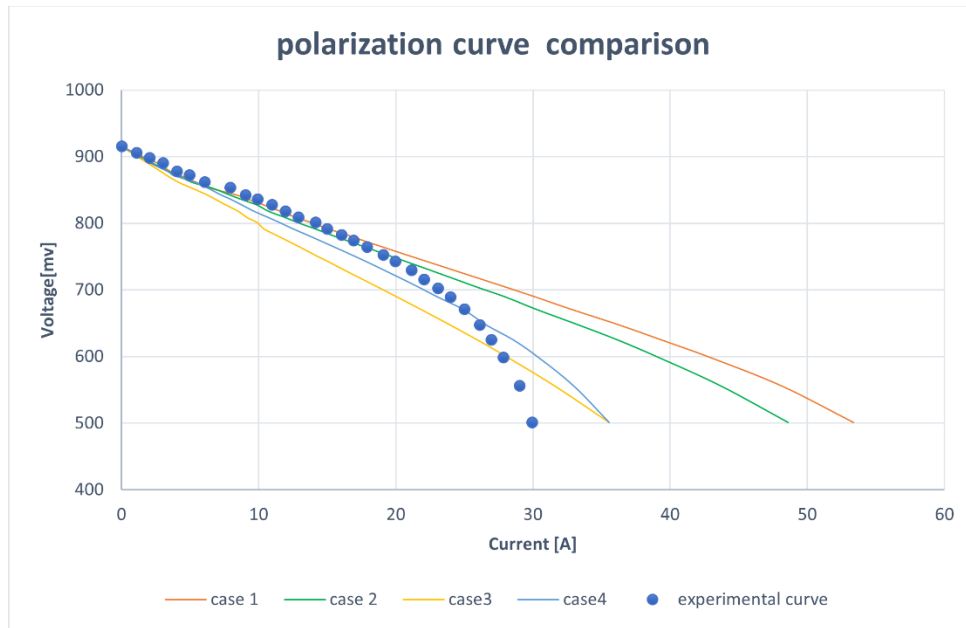


Figure 22-Fist fitting setup results

Is evident that the most similar curve is the one obtained from case 4, that is able to well represent all the three overvoltage. From this fist analysis is clear that the order of the ohmic resistance value should be in the order of magnitude of $152 \Omega/\text{cm}^2$ or lower. Not higher since the case 3 is the one that has a liner part that is not able to fit with the reference curve. The other important results is that the tortuosity should be increase and the porosity decrease, in this way the current obtained is lower and much similar to the reference value and the concentration overvoltage part of the curve is able to curve for lower values of current.

Another step is done considering the previous results modifying the fitting parameters taking into account the previous considerations. So, keeping ad best results the curve 4 and trying to optimize the results.

Case5:

T[°C]	Por.	Tort.	Rohm[Ω/cm ²]	P	Lcat[m]	Lan[m]	Lelet[m]
1173	0.15	8	0.145	1.4	35 e-6	500 e-6	5 e-6

Case6:

T[°C]	Por.	Tor.	Rohm[Ω/cm ²]	P	Lcat[m]	Lan[m]	Lelet[m]
-------	------	------	--------------------------	---	---------	--------	----------

1173	0.15	9	0.130	1.5	35 e-6	500 e-6	5 e-6
------	------	---	-------	-----	--------	---------	-------

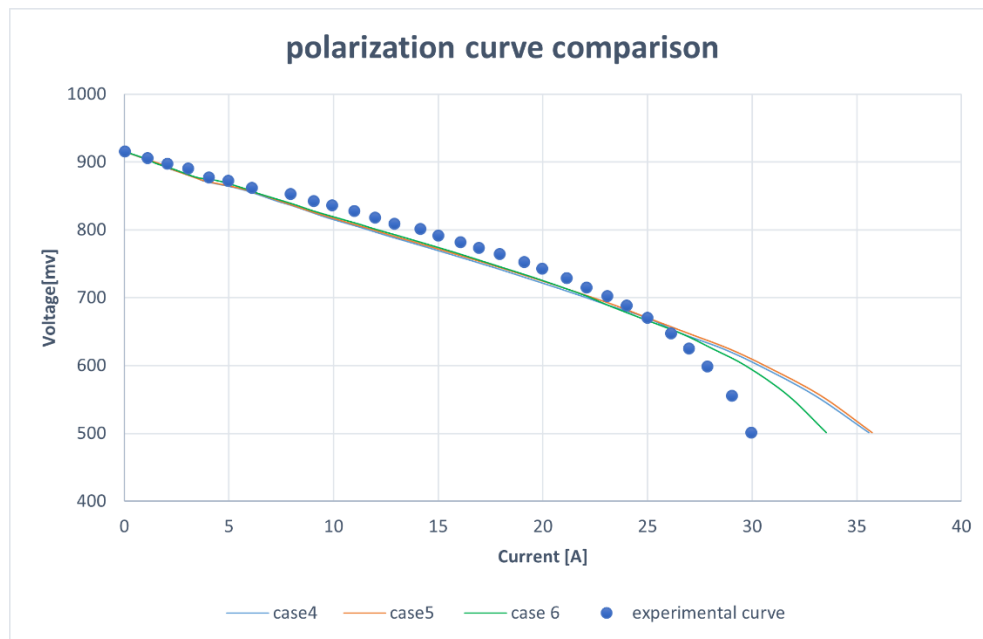


Figure 23-second fitting setup results

Between the two cases analysed the better behaviour is obtained from the cases 6.

The total number of cases analysed changing these four parameters were 14. The final results shows that the fitting value for the tortuosity is 10, for which the cell limiting current was found to be much lower, for the porosity between 0.15/0.17 and for the ohmic resistance around 0.110 Ω/cm^2 .

At the end of this procedure the three better curves are the 12 ,13 and the 14:

Case 12:

T[°C]	Por.	Tor.	Rohm[Ω/cm^2]	P	Lcat[m]	Lan[m]	Lelct[m]
1173	0.15	10	0.115	1.4	35 e-6	500 e-6	5 e-6

Case13:

T[°C]	Por.	Tor.	Rohm[Ω/cm ²]	P	Lcat[m]	Lan[m]	Lelct[m]
1173	0.17	10	0.110	1.5	35 e-6	500 e-6	5 e-6

Case14:

T[°C]	Por.	Tor.	Rohm[Ω/cm ²]	P	Lcat[m]	Lan[m]	Lelct[m]
1173	0.16	10	0.110	1.45	35 e-6	500 e-6	5 e-6

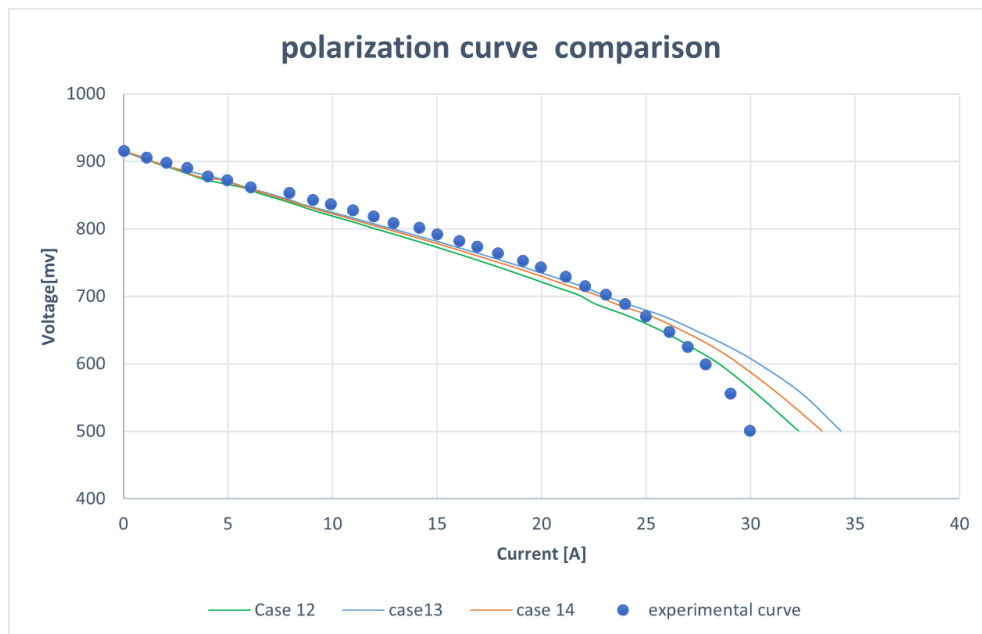


Figure 24-cases 12/13/14

Among these three the two selected are the 13 and the 14

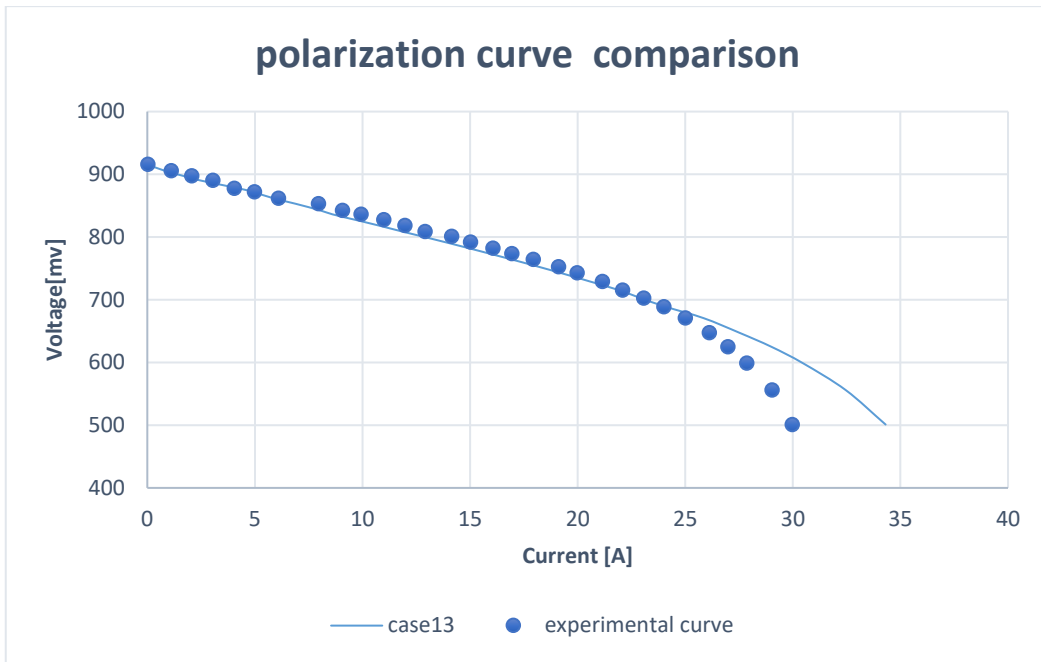


Figure 25-case 13

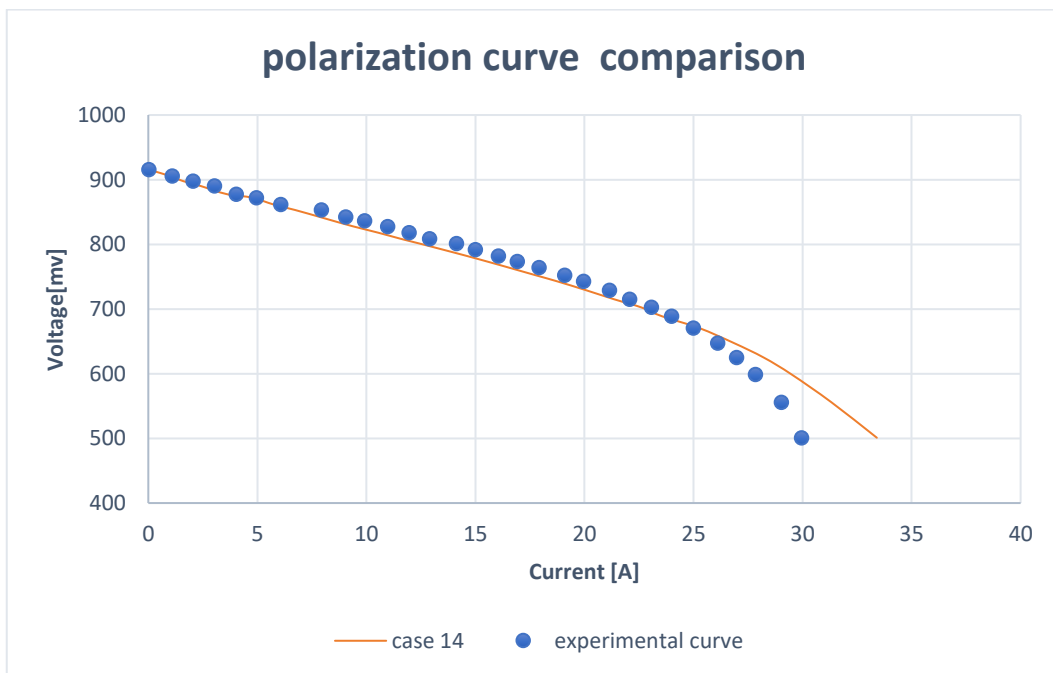


Figure 26-case 14

To properly select the correct one the standard deviation is calculated and the one with the lower value of error respect the reference one is the one that is able to represent the reference model. So according to these considerations the case 4 is the selected one. So in the following chapter where the polarization curve is obtained using as input the flow rate coming from Aspen the parameter set up is the one for case 4.

	Dev.st pop	Media.dev
<i>Case 13</i>	1.43377	1.036495
<i>Case14</i>	1.2235847	0.90180829

Table 3-Standard deviation

The comparison results are shown in table 3. It can be seen that the numerical results agree very well with experimental results. It should be noted that this validation is just utilized to examine the numerical code so that the fundamental physical parameters used in the model are applicable for SOFC settings in a general sense.

5 Aspen model

5.1 SOFC stack modeling

After the theoretical description and the mathematical model carried out using MATLAB, the SOFC module is also built using Aspen Plus.

In this part a real application is considered so the SOFC is feed with biogas, that is a mixture of carbon dioxide and methane, that can be produced from several resource and processes. The output of the SOFC are electricity and heat that can be used for different purposes.

The good aspect of this type of utilization is that no combustion is generated inside the SOFC, so in this way there is no emission of NO_x , SO_x , and particulate matter in the atmosphere.

The simulation model has been divided into five distinct parts, which are the compressions section, heating section, internal reforming, solid oxide fuel cell and heat recovery section.

1. The compression section is mainly used to increase the pressure of biogas and air with the help of F-BLOWER and AIR-BLOWER compressors respectively.
2. The heating section is adapted to preheat the biogas and air by using F-HX and AIR-HX. After that biogas will be inject towards further processing and air will inject towards the cathodic compartment of SOFC.
3. Biogas fuel of the SOFC system has been considered that consists of 60% CH_4 and 40% CO_2 and are supposed to be reformed before the SOFC's anode. In the modeling, a separate component REFORMER has been adopted.
4. SOFC section is the heart of the proposed system. It is comprised of anode, cathode and a SOFC heat exchanger and is represented by components SOFC-AN, SOFC-CATH and CATH-HX respectively.
5. The heat recovery section is composed of a burner and a couple of heaters. These components are represented by blocks named AFT-BUR, BIO-HX2, AIR-HX and F-HX and REC-HX.

The model based on existing Aspen Plus functions and unit operation models, which were used both for the fuel reformer, heat exchangers, afterburner as well as for SOFC model.

SOFC module is mainly comprised of two main components, anode, and cathode, the model of the cell is done splitting these two sides.

Peng-Robinson's (PENG-ROB) equation of state has been chosen as the base method that is suitable for modeling thermochemical gas and liquid processes at certain operating conditions within the SOFC system. Flow sheeting options in Aspen PLUS contain two useful tools that are design specifications and calculators.

A calculator block is an Aspen tool used to perform calculations with variables imported from the flowsheet or generated within the block. New variable can be exported from the block to the flowsheet. For the import variables, there are variables which are taken from the flowsheet and used inside the block. Instead, export variables, are the one which are calculated within the block and then are exported to the flowsheet.

Three calculators have been adopted for proceeding calculation of air flow rate, current produced, the molar flow rate of required oxygen delivered to the SOFC stack. These calculators enable the calculation interlinked with the modeling environment.

Moreover, to predict cell performance, two calculations were performed by implementation in the Aspen Plus additional block function using a Design-Specs module. DS is a tool that allows to define a desired set point, a target value for one variable and to define a second variable which will be changed by the DS tool, in a range defined by the user, to meet the desired set point on the first variable. One is used to calculate the amount of water recirculated from the split and the other to calculate the amount of extra air that should be sent.

The main assumptions used in the simulations are as follows:

- Fuel cell module operates at steady stage, the pressure drops in each component are neglected, all components are considered adiabatic and operating in steady state;
- The air supplied to the system is composed of 79 [%] N₂ and 21 [%] O₂, the fuel supplied to the system is biogas, CH₄ 60 [%] and CO₂ 40 [%], all chemical components are treated as ideal gases;
- The temperature of the anode and cathode outlet gases are equal to the cell stack operating temperature, the current and voltage of every cell unit are the same;
- The free Gibbs energy is minimized in all the chemical reactions and internal reforming of the biogas gains chemical equilibrium;
- The unreacted gases are assumed to be fully oxidized in the after-burner of the SOFC stack, and the after-burner is assumed to be insulation, all the heat exchangers are adiabatic;
- The proposed Aspen plus model is considered zero-dimensional.

The plant layout used for the simulations of the SOFC based generation system includes the following components: fuel and air blower, heat exchanger, mixer and split, reformer, SOFC stack characterized by separate modules for the anode and cathode, burner and recuperator. The last three components that are heat exchangers allow the heating or cooling of the fuel cell, the heat recovery from the exhausted gases and the fulfilment of thermal demand.

A schematic diagram of the SOFCs based generation system under investigation is given in the following figure-27:

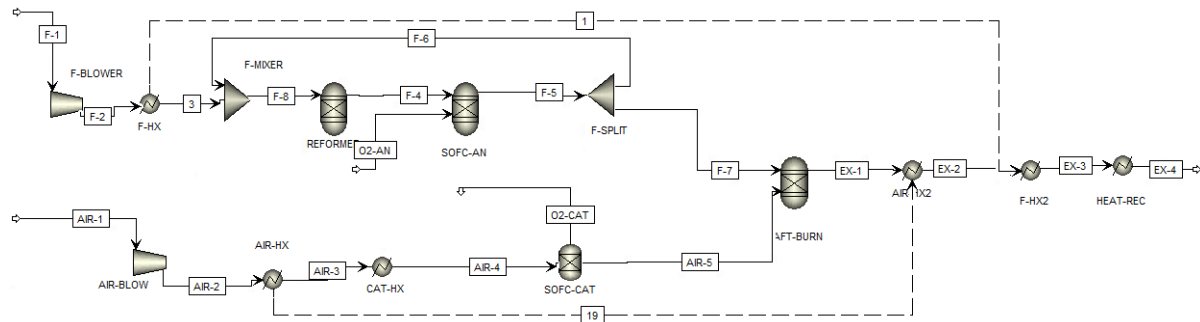


Figure 27-Aspen model

5.1 Anode side

At the inlet of the anode the fuel stream is sent at ambient temperature and pressure, 15 °C and 1 bar. At first the molar flow rate is initialized ad 1 mol/sec, then the real value needed will be overwritten thank to the calculator option, to achieve as target the total amount of currant produced by the cell using the Faraday's law taking into account the fuel utilization (FU), that is the ratio of fuel consumed within the SOFC system and fuel supplied to the SOFC. This is done inside the calculator block C-INUT. It is only a list of export variables and is created to initialize all the input data to the flowsheet. The following variable are defined:

- The fuel flow rate (biogas flow) NFUEL, is the fuel molar flow rate defined within the block according to the real value injected and exported to the flowsheet;
- The total current flowing in the SOFC system in nominal conditions CTOT, is the one produced from the available fuel flow rate according to the Faraday's law and taking into account the SOFC fuel utilization, which will be initialized. This value is exported as a PARAMETER in Aspen since it is not linked to any block or stream within the flowsheet;
- The stoichiometric oxygen flowing from cathode to anode NOXY, is the amount of oxygen requested by the SOFC electrochemical reaction (Faraday's law).

Input data:

- Volume flow rate VFUEL = 5 m³/h;
- Fuel density $\rho = 1,2 \text{ kg/ m}^3$;
- Fuel molecular weight WEIGHT = 27,2 g/mol;
- Fuel Utilization FU = 0,7;
- Faraday constant F;
- CH₄ content in biogas = 0,6;
- Charge number for CH₄ z = 4;

The equation used are :

$$m_{fuel} = v_{fuel} \cdot \rho \quad (78)$$

$$n_{fuel} = \frac{m_{fuel} \cdot 1000}{3600 \cdot WEIGHT} \quad (79)$$

$$I_{tot} = n_{fuel} \cdot 2 \cdot z \cdot F \cdot FU \cdot \%CH4 \quad (80)$$

$$n_{O_2} = \frac{I_{tot}}{4F} \quad (81)$$

In this way the oxygen flow rate introduced in the SOFC is provided. This is one of the two inlets of the SOFC, then the other is the hydrogen flow rate that is obtained from the reformer.

To summarized, Calculator C-INPUT is created to determine the molar flow rate of biogas based and the output value is exported to stream F-1 that is overwritten on it. This molar flow rate of biogas is utilized to calculate the total current produced by the SOFC system. The molar flow rate of oxygen is calculated based on Faraday's law. Also this stream is firstly initialized with 1 mol/s of oxygen. Then the real oxygen flow rate determined in the calculator is exported.

The first component is the F-BLOWER, a compressor that create a pressure increase of 200 mbar lead the pressure up to 1,2 bar with an isentropic transformation, with a mechanical efficiency of 0.8 and a thermal efficiency of 0.9.

The stream exiting the compressor is sent to the heat exchanger F-HX to be preheated up to 800°C, before to be injected in the reformer.

The next component used before the reformer is the F-MIXER, is used to model the recirculation of the exhaust fuel exiting the anode part that still contain same CH₄ and same water, with the inlet fuel.

In the reformer is important to send more water to avoid the solid carbon formation, the reformer feed must contain sufficient steam to avoid thermal cracking of the hydrocarbons and coke formation. The amount of water depends on the temperature, for higher temperatures lower amount of water are needed. To evaluate this water recirculation flow, the steam to carbon ratio (SC) is considered. This is defined as the ration between the molar flow of water over the one of methane.

$$SC = \frac{n_{H_2O}}{n_{CH_4}} \quad (82)$$

The value of the SC coefficient is calculated using Aspen Plus Define Specification function. The desired value is equal to 3 to guarantee enough water and avoid carbon deposition problems. The function is implemented considering that this value is calculated after the mixing, since at the inlet the fuel can contain same amount of water and at the outlet of the anode the exhaust gas still can contain a residual amount of methane. The variable to reach this target is the amount of water that is send back to the reformer thank the splitter component. The SC ratio equation is defined inside the DS tool using inlet methane and water to the reformer (imported from the flowsheet. The range for variable is [0-1], so the DS tool will vary the split fraction between 0 and 1 and will converge when the calculated SC will be equal to 3. Then split fraction value will be overwritten by this result.

The reformer is simulated using a Gibbs Equilibrium Reactor with a working temperature of 800°C.

The methane reformer is a type of chemical synthesis that is used to produce pure hydrogen from the methane thanks to the help of a catalyst. An Aspen Plus equilibrium reactor module RGibbs (named “REFORMER”) is selected to simulate the reforming reactions occurring inside the reformer. The methane is converted in the adiabatic reformer by catalytic partial oxidation reactions, which result in a temperature increase of the fuel gas.

Through the reaction:



This reaction is endothermic, so need thermal energy to occur. In this case the heat needed is taken from the heat available at the exit of the burner.

The anode layer is represented thought a Gibbs Equilibrium Reactor also, that is an isothermal reactor, that work at 850° C, so the operating temperature of the cell and with a pressure drop ideally null. The stream of ions O²⁻ that came from the electrolyte, is represented as an external oxygen stream, the one calculated before.

The anode and the cathode are actually not connected in the model, to allows the convergency of the system, but the stream of O₂ produced by the cathode and the one feed the anode is imposed equal. This is done through another calculator block C-OXY. One variable is NO2AN, determined inside the C-INPUT, while the second variable NO2CAT is correlated with an oxygen flow rate which is the outlet stream of separation block. Both variables are set equal in the FORTRAN code and operation is executed. In this way, the separator block is initialized with a random value of O₂ separated and then this number is overwritten.

At the end on the anode the splitter component F-SPLIT is used to separate an amount of water that is recirculated. The exhaust is sent then together to the one though the cathode is a burner to produce more heat.

5.2 Cathode side

The cathode layer is represented thanks to the separator SOFC-CAT. This component is only able to separate the oxygen from the nitrogen. In order to well simulate the cathode an artificial heat exchanger should be used, to increase the temperature of the air up to the operating temperature of the cell.

The air at ambient condition of the 15°C and 1 bar, is initially feed to a compressor AIR-BLOWER characterized by a pressure increase of 200 mbar, that increase pressure also in this case up to 1,2 bar that is the operating pressure.

Then a first heat exchanger AIR-HX is used to reach the 700 °C, the second CAT-HX is used to reach the operating temperature of the cell, so to increase the air up to 850°C. The separator produces the O₂ stream that represents the O²⁻ ions sent to the anode. The outlet of the cathode are two so the stream O₂ and the deplete air. This exhaust gases are sent together with the one exiting the anode to the burner.

Part of the exothermic heat produced is consumed in the reforming reactions in reformer block, the remaining heat is removed through the air. To know how much air is required in the cathode compartment, calculations are performed in calculator block C-AIR. The calculations are based on the first law of thermodynamics as described in the following section. The amount of heat removed by the air is expressed by the formula used is:

$$Q_{air} = m_{air} \cdot c_{p,air} (T_{out} - T_{in}) \quad (84)$$

Where $c_{p,air}$ is the heat capacity of air that is equal to 1,005 J/kgk, $T_{out}-T_{in}$ is the temperature difference of air. For this the amount of air so m_{air} that should be sent to the cathode inlet is determined

5.3 Thermal Balance

As solid oxide fuel cell operates at very high temperature, therefore there is a thermal exchange between the cell and the external environment. So, thermal balance on the SOFC is applied based on the first law of thermodynamics. This balance considers all the heat sources and heat sink caused by electrochemical reactions within the stack.[27]

The amount of air that is sent at the inlet of the cathode side is evaluated considering the thermal balance. This value is not equal to the stoichiometric one because an extra amount of air is needed to then cool down the system. The outputs of the cell are electrical power W_{el} and thermal heat flux Φ . In the SOFC mode the heat is produced and so according to the sign convention is negative, so the heat flux is obtained through the formula:

$$|\Phi| = |\Delta H_{reac}| - W_{el} \quad (85)$$

ΔH_{reac} is the enthalpy change across the anode; this is not all going into heat. But this goes partially into electricity production and the remaining part will go to heat

Explicating the terms:

$$|\Phi| = |\Delta H| \cdot n_{H_2} - V_c \cdot I_{tot} \quad (86)$$

Using the Faraday's law to express the hydrogen molar flow and considering the total current as the one produced by a single cell multiplied by the number of cells:

$$|\Phi| = |\Delta H| \cdot \frac{In_{cell}}{2F} - V_c \cdot In_{cell} \quad (87)$$

So :

$$|\Phi| = In_{cell} \left(\frac{|\Delta H|}{2F} - V_c \right) \quad (88)$$

The total heat flux is the sum of the contribution given by the reform, so the heat needed for the reaction to occur and this is given by Aspen, and the heat that should be removed by the air.

$$|\Phi| = \Phi_{air} + \Phi_{REF} \quad (89)$$

Φ_{ref} is the heat flux required to process endothermic reforming reactions, Φ_{air} is the quantity of heat flux that is removed by air and is equivalent to:

$$\Phi_{air} = \Phi - \Phi_{REF} \quad (90)$$

Evaluating the Φ_{air} from this equation the mass of air can be obtained:

$$\dot{m}_{air} = \frac{\Phi_{air}}{c_p(T_{out,air} - T_{in,air})} \quad (91)$$

Also this step is implemented in aspen thank to the calculator option C-AIR. The calculator block solves the thermal balance and calculate the waste heat which should be removed by the air flow.

$$\Phi_{waste} = \Phi_{air} \quad (92)$$

Inside the calculator block the electrical power is evaluated considering the formula:

$$W_{el} = V_c \cdot I_{tot} \quad (93)$$

Where the I_{tot} is given from the previous calculations.

Put all together:

$$\Phi_{waste} = \Phi_{air,real} = \Phi - \Phi_{REF} = \Delta H_{reac} - W_{el} - \Phi_{REF} \quad (94)$$

This value is then exported as a PARAMETER to be used in the following design specification DS-AIR.

Here, the target is that the two heat fluxes are equal, the waste and the heat duty of the cathode heat exchanger.

$$\Phi_{waste} = \Phi_{HXcat} \quad (95)$$

The variable to reach the target is the inlet air flow, that will be varied keeping the temperature of the SOFC constant and to remove the heat produced.

This is expressed as a function of the stoichiometric air thanks to the lambda coefficient that is assumed variable between 1 and 20.

$$\lambda = \frac{n_{air,real}}{n_{air,stoich}} \quad (96)$$

λ is the air excess ratio or also called air utilization. $n_{air,stoich}$ represents stoichiometric air in kg/sec and is calculated by using Faraday's law, so considering how much oxygen as required to obtain n_{O_2} . Therefore, in this way, the air excess ratio with respect to stoichiometric air is determined from the thermal balance of the SOFC system.

5.4 Aspen Results

Aspen given as results:

To evaluate the system performance, the efficiencies calculation considering the different component are performed. Efficiency determined are:

- DC electrical power from the SOFC,
- Air and biogas blowers' electrical consumption,
- Useful thermal power from the system,

These outputs are used to evaluate the system performance through the efficiencies calculation considering the different component are performed. Efficiency determined are:

- Electrical efficiency,
- Thermal efficiency,
- Overall efficiency,

The definitions are:

$$\eta_{electrical} = \frac{W_{net}}{m_{fuel} \cdot LHV} \quad (97)$$

$$\eta_{thermal} = \frac{Q_{REC}}{m_{fuel} \cdot LHV} \quad (98)$$

$$\eta_{overall} = \frac{W_{net} + Q_{REC}}{m_{fuel} \cdot LHV} \quad (99)$$

$\eta_{\text{Electrical}}$ represents the electrical efficiency of the system, W_{net} symbolizes the total electrical power output (kW) and is evaluated in this way:

$$W_{\text{net}} = W_{\text{net,AC}} = W_{\text{gross,,AC}} - W_{\text{AUX}} = W_{\text{gross,DC}} \cdot \eta_{\text{inv}} - W_{\text{air,blow}} - W_{\text{fuel,blow}} \quad (100)$$

Where η_{inv} is the efficiency of the inverter, and the $W_{\text{air,blow}}$ and $W_{\text{fuel,blow}}$ are the power consumed by the compressor to increase the pressure for the air and the fuel.

η_{Thermal} represents the thermal efficiency. Q_{REC} denotes the extra heat recovered from the heat recovery system. η_{Overall} is the overall efficiency of the system, considering both of them.

Using as $v_{\text{fuel}} 5 \text{ m}^3/\text{h}$ the results obtained for Aspen are:

For the cathode:

	<i>Units</i>	<i>AIR-4</i>
<i>Mole flows</i>	mol/s	0.206281
<i>CH4</i>	mol/s	0
<i>CO2</i>	mol/s	0
<i>N2</i>	mol/s	0.162962
<i>CO</i>	mol/s	0
<i>O2</i>	mol/s	0.0433191
<i>H2O</i>	mol/s	0
<i>H2</i>	mol/s	0

Table 4-Cathode flow rates

In this case at the cathode just air is sent and so the two components present are the oxygen and the nitrogen, with the molar flow rate resulting from the calculation.

For the anode:

	<i>Units</i>	<i>F-4</i>
<i>Mole flows</i>	mol/s	0.258689
<i>CH4</i>	mol/s	7.34257 e-5
<i>CO2</i>	mol/s	0.0525563
<i>N2</i>	mol/s	0
<i>CO</i>	mol/s	0.0650214
<i>O2</i>	mol/s	5.28372 e-20
<i>H2O</i>	mol/s	0.0598783
<i>H2</i>	mol/s	0.0811594

Table 5-Anode flow rates

For the anode the stream considered is the one exits the reformer and entering the anode side, so the methane residual is very low since was converted in the previous step, the hydrogen is the one considered as a fuel for the SOFC, while the carbon monoxide and dioxide are the diluent, that in the code are assigned in the $N_{2diluent}$.

These flow rates are used as input for the MATLAB code. The proper conversion is done to obtain them in Nml/min.

	<i>Flow rate [Nml/min]</i>
H_2	1090,782
H_2O	804,7644
$N_{2diluent}$	1580,244
<i>Air</i>	2772,417

Table 6-Flow rate values

From these values the code is able to perform the current density calculation from which the polarization curve as in the case before is evaluated.

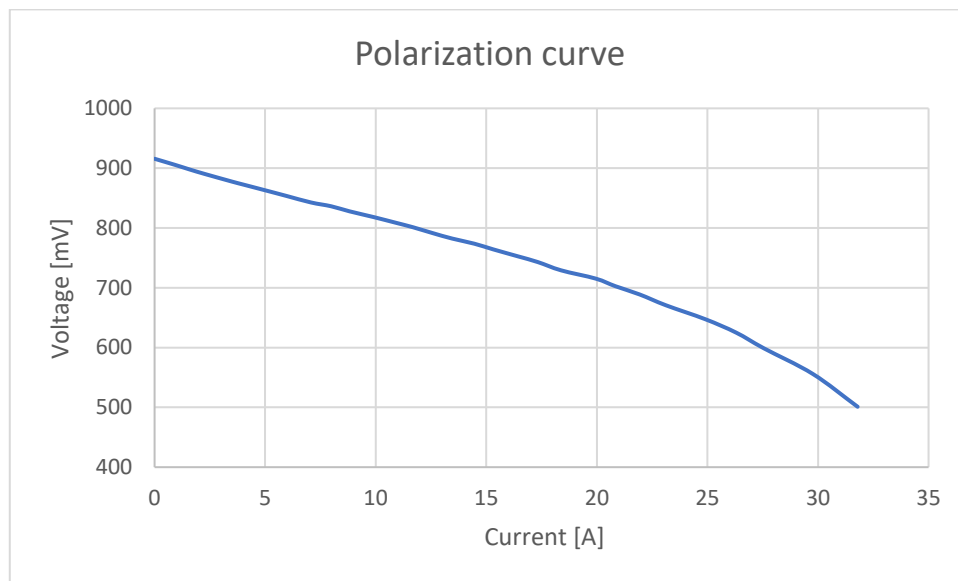


Figure 28- Polarization curve from Aspen results

The thermal and electrical outputs instead are summarised in the table below:

	<i>Variable in [W]</i>
Q_{waste}	1033,77
Q_{rec}	-15687,6
W_{el}	9535,99
$W_{airblow}$	128,378
$W_{fuelblow}$	22,6894

Table 7-Aspen results

From these values is possible to make the efficiency evaluation. The electrical power as results of Aspen is the $W_{DC,gross}$, so using the formula (100), with an efficiency for the inverter of 0.95, the net power is calculated. The mass fuel flow rate is given by the expression (78) and the lower heating values for the methane is $LHV= 50.0$ MJ/kg.

The results are:

<i>Efficiency</i>	
$\eta_{electrical}$	0,188101
$\eta_{thermal}$	0,106812
$\eta_{overall}$	0,2949127

Table 8- Efficiency

6 Conclusion

A mathematical model was developed to study the behaviour of a SOFC. An anode-supported planar one-dimensional SOFC stack model has been presented. The model developed consists of mass and energy balances, and an electrochemical model that relates the fuel and air gas flow and temperature to voltage, current density, and other relevant fuel cell variables.

Mass transport of gas components through porous anode was investigated using the Dusty Gas Model. The performance of cell polarization, is separated in different polarization losses, including the ohmic resistance, activation polarization, concentration polarization. The model was validated by comparing the simulation results with data from literature and good agreement between them was found, changing the fitting parameter.

The model can effectively predict the I–V characteristics of SOFC, and the distributions of gas molar fraction inside the porous electrodes. It was concluded that the diffusion process across porous medium can be managed by operating conditions together with microstructural properties of material.

References

- [1] [GOAL 13: Climate action | UNEP - UN Environment Programme](#)
- [2] [Causes of climate change \(europa.eu\)](#)
- [3] [SR15 Chapter 1 HR.pdf \(ipcc.ch\)](#)
- [4] [World Energy Outlook 2021 \(windows.net\)](#)
- [5] [NetZero by 2050 - A Roadmap for the Global Energy Sector CORR.pdf](#)
- [6] [Renewable Power – Analysis - IEA](#)
- [7] [Global Energy Review CO2 Emissions in 2021.pdf](#)
- [8] Nur Syafkeena Mohd Affandi, Nafisah Osman, Short review on global trends in SOFC scenario and future perspective, *Materials Today: Proceedings*, 2022
- [9] F. Calise, F.L. Cappiello, L. Cimmino, M. Vicidomini, Dynamic simulation modelling of reversible solid oxide fuel cells for energy storage purpose, *Energy*, Volume 260, 2022
- [10] Chen Kele, Wang Xinmei, Naser Youssefi, Model parameter estimation of SOFCs using a modified cat optimization algorithm, *Sustainable Energy Technologies and Assessments*, Volume 52, Part B, 2022
- [11] Guoping Xu, Zeting Yu, Lei Xia, Changjiang Wang, Shaobo Ji, Performance improvement of solid oxide fuel cells by combining three-dimensional CFD modeling, artificial neural network and genetic algorithm, *Energy Conversion and Management*, Volume 268, 2022
- [12] Weidong He, Jing Zou, Bin Wang, Subramanian Vilayurganapathy, Ming Zhou, Xiao Lin, Kelvin H.L. Zhang, Junhao Lin, Ping Xu, James H. Dickerson, Gas transport in porous electrodes of solid oxide fuel cells: A review on diffusion and diffusivity measurement, *Journal of Power Sources*, Volume 237, 2013, Pages 64-73, ISSN 0378-7753
- [13] Fatma N. Cayan, Suryanarayana R. Pakalapati, Francisco Elizalde-Blancas, Ismail Celik, On modeling multi-component diffusion inside the porous anode of solid oxide fuel cells using Fick's model, *Journal of Power Sources*, Volume 192, Issue 2, 2009, Pages 467-474, ISSN 0378-7753
- [14] Fu, Y., Y. Jiang, S. Poizeau, A. Dutta, A. Mohanram, J. D. Pietras, and M. Z. Bazant. "Multicomponent Gas Diffusion in Porous Electrodes." *Journal of the Electrochemical Society* 162, no. 6 (March 23, 2015): F613–F621.
- [15] Penyarat Chinda, Somchai Chanchaona, Pascal Brault, Wisanuruk Wechsato. Mathematical Modeling of a Solid Oxide Fuel Cell with Nearly Spherical-Shaped Electrode Particles. *Journal of Sustainable Energy and Environment*, 2010, 1, pp.185-196. fhal-00581564f
- [16] Pianko-Oprych, Paulina & Palus, Mateusz. (2017). Simulation of SOFCs based power generation system using Aspen. *Polish Journal of Chemical Technology*. 19. 10.1515/pjct-2017-0061.

- [17] Ahmed, K., Amiri, A., & Tadé, M. O. (2020). Simulation of Solid Oxide Fuel Cell Anode in Aspen HYSYS—A Study on the Effect of Reforming Activity on Distributed Performance Profiles, Carbon Formation, and Anode Oxidation Risk. *Processes*, 8(3), [268].
<https://doi.org/10.3390/pr8030268>
- [18] [IRENA Global Renewables Outlook 2020.pdf](#)
- [19] [2020 was one of three warmest years on record | World Meteorological Organization \(wmo.int\)](#)
- [20] [Path-to-Hydrogen-Competitiveness_Full-Study-1.pdf](#)
- [21] [The_Future_of_Hydrogen.pdf](#)
- [22] [IRENA World Energy Transitions Outlook 2022.pdf](#)
- [23] [IRENA Geopolitics Hydrogen 2022.pdf](#)
- [24] [FCT - Fuel Cell Technologies - SOFC \(archive.org\)](#)
- [25] Lishan Peng, Zidong Wei, Catalyst Engineering for Electrochemical Energy Conversion from Water to Water: Water Electrolysis and the Hydrogen Fuel Cell, *Engineering*, Volume 6, Issue 6, 2020, Pages 653-679, ISSN 2095-8099
- [26] Bo Yang, Jingbo Wang, Mengting Zhang, Hongchun Shu, Tao Yu, Xiaoshun Zhang, Wei Yao, Liming Sun, A state-of-the-art survey of solid oxide fuel cell parameter identification: Modelling, methodology, and perspectives, *Energy Conversion and Management*, Volume 213, 2020, 112856, ISSN 0196-8904
- [27] Muhammad Ishaq, Haris Ishaq, Performance assessment of biogas-fed solid oxide fuel cell system for municipal solid waste treatment, *Journal of Cleaner Production*, Volume 354, 2022, 131702, ISSN 0959-6526
- [28] J. Laurencin, D. Kane, G. Delette, J. Deseure, F. Lefebvre-Joud, Modelling of solid oxide steam electrolyser: Impact of the operating conditions on hydrogen production, *Journal of Power Sources*, Volume 196, Issue 4, 2011, Pages 2080-2093, ISSN 0378-7753
- [29] Andrea Lanzini, Pierluigi Leone, Experimental investigation of direct internal reforming of biogas in solid oxide fuel cells, *International Journal of Hydrogen Energy*, Volume 35, Issue 6, 2010, Pages 2463-2476, ISSN 0360-3199
- [30] Paola Costamagna, Paolo Costa, Vincenzo Antonucci, Micro-modelling of solid oxide fuel cell electrodes, *Electrochimica Acta*, Volume 43, Issues 3-4, 1998, Pages 375-394, ISSN 0013-4686
- [31] M.M. Hussain, X. Li, I. Dincer, Mathematical modeling of transport phenomena in porous SOFC anodes, *International Journal of Thermal Sciences*, Volume 46, Issue 1, 2007, Pages 48-56, ISSN 1290-0729
- [32] Grzegorz Brus, Kosuke Miyawaki, Hiroshi Iwai, Motohiro Saito, Hideo Yoshida, Tortuosity of an SOFC anode estimated from saturation currents and a mass transport model in comparison with a real micro-structure, *Solid State Ionics*, Volume 265, 2014, Pages 13-21, ISSN 0167-2738
- [33] [TESI_FERRERO.pdf](#)

[34] Xiaoqiang Zhang, Mayken Espinoza, Tingshuai Li, Martin Andersson, Parametric study for electrode microstructure influence on SOFC performance, International Journal of Hydrogen Energy, Volume 46, Issue 75, 2021, Pages 37440-37459, ISSN 0360-3199

[35] SYNTHESIS, CHARACTERIZATION AND COMPARATIVE STUDY OF LSCM AND Ce-SUBSTITUTED LSCM ANODE POWDERS FOR APPLICATION IN SOLID OXIDE FUEL CELLS - Scientific Figure on ResearchGate. Available from: https://www.researchgate.net/figure/Schematic-diagram-for-a-planar-SOFC-design-23_fig2_331024790 [accessed 1 Oct, 2022]